Modeling of biomass char gasification, combustion, and attrition kinetics in fluidized beds

Richard B. Bates[1*], *Christos Altantzis*[1,2], *Ahmed F. Ghoniem*[1]

1 Department of Mechanical Engineering, Massachusetts Institute of Technology 77 Massachusetts Avenue, Cambridge, MA 02139-4307, USA

2 National Energy Technology Laboratory, 3610 Collins Ferry Road, Morgantown, WV 26507, USA

Abstract

Char conversion is one of the most pivotal factors governing the effectiveness of fluidized bed gasification systems. Gasification-assisted attrition is a phenomenon whereby heterogeneous reactions progressively weaken a char's structure throughout its lifetime leading to enhanced attrition and the production of a significant fraction of fines that exit the reactor unconverted. While this effect has been observed and measured experimentally, few models have been developed to quantitatively account for it, particularly for biomass chars. In this study, a transient gasification and combustion particle model is presented to describe primary fragmentation, attrition, and heterogeneous reactions of a single batch of particles. A conversion-dependent structural function is proposed to describe gasification-assisted attrition and the model parameters are fitted to published experimental data ref [2]. The fragile structure of char derived from wood chips contributes to a higher initial attrition rate than char from wood pellets, but the hardness of both feedstocks is shown to deteriorate rapidly as they convert. A

shrinking particle combustion model which accounts for variable feedstock properties is comprehensively presented and validated against the aforementioned data set. The combustion behaviors of both feedstocks are found to strongly depend on particle size/geometry because of significant mass transfer limitations. Using a residence time distribution approach, the model is extended to describe a continuously fed system in order to examine the sensitivity of steady state outputs (conversion and residence time) to the operating temperature, pressure, and kinetics. As the temperature increases, the char reactivity also increases but the coupled and competing effect of gasification-assisted attrition acts to shorten the residence time of the char particles making complete char conversion very difficult even at 900°C- the upper operating temperature limit for most single stage fluidized bed gasification systems. Low operating temperatures result in longer average residence times and higher steady-state char inventories, and slower kinetics lowers the overall conversion. Because of inhibition effects, elevated operating pressures have a smaller impact on improving conversion compared to higher temperature. The steady model further provides a rigorous method for estimating the maximum stable biomass feeding rates as a function of relevant independent parameters including reactor temperature, pressure, volume, and feedstock characteristics.

1. **Introduction**

Because of rising concerns over greenhouse gas emissions and regulatory production mandates, alternatives to traditional fossil-derived transportation fuels are receiving much attention. Fluidized bed biomass gasification (FBBG) is a promising technology for the thermochemical conversion of lignocellulosic biomass to second generation renewable fuels. Owing to the high rates of heat/mass transfer and the thermal inertia of the bed material, fluidized bed reactors can be used to process a wide variety of feedstocks with minimal preparation. After appropriate gas cleanup, the syngas produced by gasification can be utilized in an already-commercialized catalytic Fischer-Tropsch process to produce drop-in diesel or combusted to generate electricity.

The reactive environment of a fluidized bed gasifier is characterized by a number of complex physical and chemical processes occurring over a range of time-scales[1]. During FBBG, raw biomass fed into a fluidized bed of inert granular material, initially undergoes rapid mixing, heating, drying, and devolatilization which results a mixture of light and condensable gases (pyrolysis products) as well as highly porous carbonaceous char- the latter further reacts with steam and carbon dioxide to produce syngas. A portion of the char may also combust with oxygen, generating heat to drive the endothermic gasification reactions. Because of the abrasive and chaotic environment of the fluidized bed, the fragile char particles experience mechanical effects such as attrition and secondary fragmentation which produce fines that can be blown out of the reactor, unconverted.

FBBG faces several technical hurdles to achieve commercialization. Because of the melting and agglomeration tendencies of the alkali/alkaline metals contained in biomass ash, the maximum operating temperatures are usually limited to less than 900°C[2]. The relatively low

operating temperature results in the formation and growth of condensable tars in the product syngas (2-50 g/Nm^3)[3] as well as incomplete conversion of the char. Depending on the end application, the significant methane fraction must also be subsequently reformed. These three issues remain as major hurdles to further commercialization of the technology[4].

In particular, char conversion has been shown to be a pivotal, rate-limiting step, which governs many performance metrics of a gasifier including its operating temperature, the heating value of the product syngas, and the overall cold gas efficiency[5]. According to Thunman and Seeman [6] around 50-80% of the char exits the gasifier unconverted during single-stage FBBG. Recycling the unconverted char appears to improve conversion[7] and a variety of more complex multi-stage gasification systems have been proposed to ameliorate this issue[8].

Despite the importance of this phenomena to the overall effectiveness of the process, many existing reactor models resort to semi-empirical correlations or simply assume a degree of conversion [9]. The difficulty in robustly predicting carbon conversion is related to various highly-feedstock dependent physico-chemical processes affecting char. First, there is large variability in the reactivity of biomass char depending on the feedstock and heating conditions[10]. Reactivity refers to the rates (1/s) of gasification and combustion reactions under kinetically limited conditions,

$$C + H_2O \leftrightarrow H_2 + CO \text{ (+131.4 kJ/mol)} \quad (1)$$

$$C + CO_2 \leftrightarrow 2CO \text{ (+172.5 kJ/mol)} \quad (2)$$

$$C + 0.5O_2 \rightarrow CO \text{ (-393.8 kJ/mol)} \quad (3)$$

Second, the reactivity itself can either increase or decrease[11] significantly throughout the conversion- phenomena attributed to the catalytic impact of the ash and changes in the pore morphology[12]. The latter is usually accounted for using some form of semi-empirical structural

profile model (e.g. the random pore model RPM) requiring additional parameters. Third, the rate-inhibiting effects of small quantities of hydrogen and carbon monoxide (<30% vol.) are extremely significant especially at higher operating pressures[13]. This necessitates the fitting of Langmuir-Hinshelwood (LH) kinetics parameters. Lastly, gasification-assisted attrition is a phenomenon whereby the heterogeneous steam and Bouduard reactions progressively weaken the char structure throughout its conversion leading to enhanced attrition. While this effect has been observed and recently measured experimentally[14], no models were developed to describe it in that study. Troiano et al. recently proposed a model for gasification-assisted attrition of lignite char[15] which demonstrated an exponential dependence on carbon conversion degree. However, it required a fitting parameter based on the number of secondary fragments generated. To summarize, biomass char gasification reactivity and attrition kinetics exhibit feedstock and conversion dependent behavior, and models and parameters are lacking to comprehensively account for these effects.

A summary of the state of the art biomass char gasification and combustion kinetics models is given in Table 1. A key differentiating factor between kinetics models is their treatment of the average, steady state residence time $\bar{\tau}_{char,ss}$ of the char particles[16],

$$\bar{\tau}_{ch,ss} = m_{ch,ss}/(\dot{m}_f Y_{ch}) \quad (4)$$

where $m_{ch,ss}$ is the char inventory of the bed at steady state in kg_{char}, $\dot{m}_f$ is the feed rate in $kg_{biomass}$/sec and Y_{ch} represents the char yield after devolatilization in $kg_{char}/kg_{biomass}$. The denominator represents the steady-state feeding rate of char into the gasifier and can be computed from known variables. Meanwhile the char inventory at steady state is neither independently controllable nor easily measured and therefore is usually unknown. Kotinnen et al.[17] measured reactivity using thermogravimetric analyzer (TGA) experiments to fit LH kinetics

and explored the impact of char residence time on char conversion. Instead of assuming a single residence time for all particles, Nilsson et al. assumed a well-stirred residence time distribution (RTD), applied power-law kinetics rate expressions, and neglected attrition effects[18]. There is limited predictive capability from either of these models because the average residence time is defined by the char inventory of the bed which is not known *a priori*. Gomez-Barea and Leckner (GB&L)[5] incorporated the effects of primary fragmentation, attrition of fines, and reactivity to iteratively compute steady-state char inventory (and therefore residence time); however, they do not account for the impact of varying particle size or conversion level on the attrition rates. The model of Kramb et al.[19] applied a complex structural profile model (hybrid random pore model) to the GB&L model requiring fitting of additional parameters. Recently, Natale et al.[20] developed a transient population balance model (PBM) which considers mother particles to produce a size distribution of fines which themselves continue to react and eventually elutriate. However, the effects of gasification assisted attrition were not accounted for.

Table 1 Comparison of existing kinetics models for char gasification and combustion

	Mean residence time $\overline{\tau}_{char}$	**Gasification kinetics mechanism**	**Attrition model**	**Reactivity/ structural model: Gasification**	**Reactivity/ structural model: Combustion**
Scala and Salatino, 2002[21]	Solved from material balance	(NC)	Fixed, average particle diameter and attrition rate	(NC)	SUPM
Khan et al., 2007 [22]	Discrete population balance	(NC)	Diameter dependent attrition rate	(NC)	SUPM
Kaushal et al., 2010[23]	Computed (iteratively)	Power-law	(NC)	SUPM	(NC)
Kontinnen et al. 2012[17]	Assumed (1-10000 sec)	Langmuir-Hinshelwood	(NC)	UCM	(NC)
Nilsson et al., 2012[18]	12 minutes, well-mixed distribution	Power-law	(NC)	UCM	SUCM
Gomez-Barea and Leckner, 2013[5]	Computed (iteratively)	Power-law	Fixed, average particle diameter and attrition rate	UCM	SUCM
Kramb et al., 2014[19]	Computed (iteratively)	Langmuir-Hinshelwood	(Taken from experiment)	HRPM	(NC)
Natale et al., 2014[20]	Computed (transient population balance)	(Not specified)	Attrition model for mother particles,	SUPM	SUPM

Abbreviations: *SUPM- shrinking unreacted particle model, UCM- uniform conversion model; HRPM- hybrid random pore model, SUCM- shrinking unreacted core model; (NC), not considered*

Comparing existing work, many do not explicitly describe the impact of attrition/elutriation and -of the ones that do- none have attempted to incorporate the effects of gasification-assisted attrition. Additionally, char combustion is not necessarily described by all the models, limiting their applicability to oxygen-free gasification conditions. Of the models that do consider char combustion, it is sometimes unclear on whether or how internal mass transfer limitations are accounted for. In some cases, several adjustment parameters for the mass transfer coefficient and combustion reactivity are used[20,24]. As result, it is difficult to utilize these models for feedstock besides those used in the original modeling. In particular, no models have been fitted to describe pelletized feedstocks which have higher char density and thus demonstrate significantly different conversion characteristics under both gasification and combustion conditions compared to raw biomass[14].

In order to address these issues, this work proposes a new conversion-dependent function to describe gasification-assisted attrition, the parameters of which are fitted from published experimental data of batch fluidized bed gasification/attrition experiments of spruce wood pellets and pine wood chips[14]. In order to carry out this fitting procedure, a transient gasification model describing the primary fragmentation, attrition, and heterogeneous reactions of a batch of particles is developed (sections 2.1 and 2.2). Additionally, a rigorous combustion model accounting for external/internal mass transfer and kinetic limitations is described in section 2.3. The estimation and impact of internal diffusion limitations on the char combustion rate is formally presented, which are shown to explain significant differences between feedstocks. The fitting and validation of the transient gasification and combustion model is shown in sections 3.1 and 3.2, respectively. Through suitable residence time distribution (RTD) averaging of the transient results, the model is extended to describe steady state results for a continuously fed

system in section 3.3. Last, practical implications for fluidized bed gasifier operation are supported by a discussion on the overall sensitivity of carbon conversion to temperature, pressure, fitted, and input parameters.

2. **Mathematical model**

The objective of the transient char particle model is to describe the chemical and physical conversion of char and attrited fines as a function of time subjected to a specified gasification environment (temperature, pressures, gas phase species concentrations). Since the gas composition is required as an input, it can come from experimental measurements or a separate sub-model which solves steady-state homogeneous gas phase reaction kinetics in the fluidized bed[25]. FBG is complicated process involving thousands of largely independent reacting particles so the development of appropriately justified simplifications is necessary[1]. A time-scale analysis[1] whose assumptions and results are summarized in Table 1 aids in identifying the relevant physical and chemical processes affecting biomass char. Many of the time-scale definitions are derived in the Appendix or later in this text, while the assumptions for the bed geometry and conditions are from those used in Ammendola et al. [14].

Table 2 Characteristic times of physical and chemical processes during fluidized bed gasification of biomass char

	Characteristic time in seconds	
	T= 1073K P=101325Pa	
Transport process or reaction	Coarse particles d_{ch}=1mm	Fine particles d_{ch} =50μm
Intraparticle diffusion, $d_{ch}{}^2/(36D_{eff})$	9*10^{-4}	2*10^{-6}
External mass transfer to particle, $d_{ch}^2/(6ShD_{binary})$	6.6*10^{-4}	1.7*10^{-6}

Combustion kinetics time scale (intrinsic), $1/(k_{O_2} C_c \lambda)$		4.4*10^{-4}	
Internal effectiveness factor, η_{int}	0.53 [-]		1 [-]
External effectiveness factor, η_{ext}	0.55 [-]		1 [-]
Combustion time scale (overall) $1/R_{comb}$	100		30
Steam gasification time scale, $1/R_{H_2O}$		720	
Carbon dioxide gasification scale, $1/R_{CO_2}$		750	
Elutriation time scale $1/R_{elu}$	Inf (u_t<u_0)		4

Physical properties and correlations	
Gas phase composition	X_{O_2}=0.01 X_{CO_2}=0.2 X_{H_2O}=0.2
Gas phase properties	$D_{eff} = 3 * 10^{-5}$ m^2/sec D_{binary} =1.8*10^{-4} m^2/sec ρ_f = 0.329kg/m^3 μ_f =4.6*10^{-5} Pa s
Bed material properties	$d_p = 350 * 10^{-6}$m ρ_p = 2600kg/m ρ_{ch}=100 kg/m^3
Bed properties	d_{bed} = 0.04m m_{bed} = 0.18kg A_{bed} = 0.001256m^2
Superficial, minimum fluidization velocity (m/s)	u_0 = 0.8 m/s u_{mf} = 0.0438m/s
Terminal velocity (m/s) [26]	$u_t = \frac{\mu_f}{d_{ch}\rho_f}\left(\sqrt{27^2 + 3Ar} - 27\right)$ $Ar = \rho_f(\rho_{ch} - \rho_f) g {d_{ch}}^3/{\mu_f}^2$ g = 9.8 m/sec^2
Elutriation rate (1/s), coarse particles[27]	$R_{elu,coarse}$ = $0.011\rho_{ch}(1 - u_t/u_0)^2 A_{bed}/m_{bed}$ if $u_0 < u_t$, $R_{elu,coarse}$ = 0
Elutriation rate (1/s), fine particles (<74 μm) [28]	$R_{elu,fines} = 9.43 * 10^{-4}\rho_f u_0 \left(u_0^2/g d_p\right)^{1.65} A_{bed}/m_{bed}$
Char combustion properties	$C_c \approx$ 15,000 mol$_C$/m^3 λ =0.5

Some important conclusions can be drawn from this analysis. Namely, gasification reactions are generally much slower than mass transport processes. However, combustion of coarse particles (~1mm) exhibits a much faster rate than gasification and is subject to significant mass transfer limitations. This causes the internal and external effectiveness factors (defined in the Appendix) to be less than unity. While commonly neglected[29], this analysis shows that the significant internal diffusion resistance must actually be included when modeling the combustion of millimeter sized char particles. Fines are sufficiently small so they do not experience mass transfer limitations under either gasification or combustion conditions. The terminal velocity of the coarse particles is higher than the superficial gas velocity, so according to the model

proposed by Colakyan and Levenspiel[27] their elutriation rate is negligible. Meanwhile, the fines are expected to be elutriated rapidly in a matter of a few seconds under these conditions.

As demonstrated in Figure 1, the model considers two classes, mother particles produced by devolatilization and primary fragmentation, and fines produced by the abrasion of mother particles. This two-class description was originally proposed by models for fluidized bed combustion of coal[16,30] and can be assumed when the number of intermediate-sized particles is small or zero[20,22,31]. Secondary fragmentation of biomass chars derived from spruce pellets and wood chips under combustion conditions generates relatively few (~2.5-3) fragments per original char particle, and appears to be largely independent of the oxygen concentration[32,33]. On the other hand, fluidized bed gasification of lignite char appears to generate a large number of fragments (>70) and depends on the operating conditions[15]. Unfortunately, there is a lack data, models, and parameters to quantitatively include the impact of secondary fragmentation of biomass chars under gasification conditions.

For the gasification reactions, internal and external mass transfer processes are fast compared to chemical kinetics[1,18], so the gasification reactions of the mother particles can be assumed to occur uniformly- meaning that no species concentration or thermal gradients exist within the particle. Referred to as the uniform conversion model (UCM), shrinkage/expansion due to gasification is neglected; however, abrasion of the mother particles occurs at the exterior surface and acts to reduce their average diameter. Fines produced by attrition are assumed to be elutriated as soon as they are produced. This assumption is valid under oxygen-free gasification conditions because the residence time of the fines is small (a few seconds) compared to the time-scale of their chemical reaction[1,20].

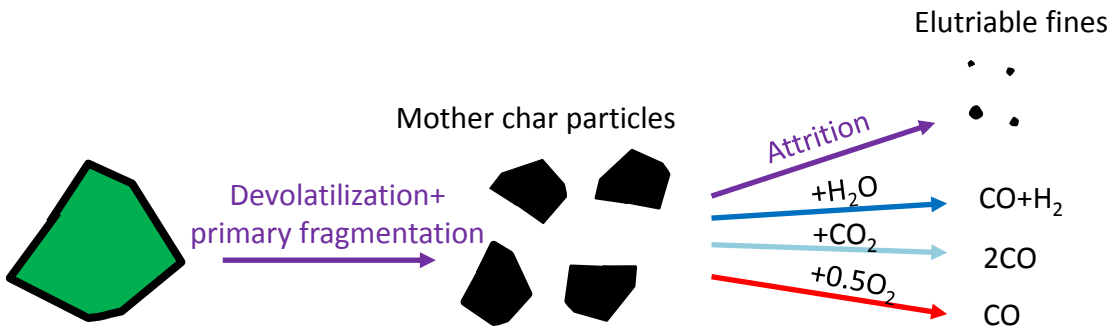

Figure 1 Schematic showing main physical and chemical processes considered in the char conversion model

Under combustion conditions, the time-scales of chemical reaction are shorter than those of gasification[1], thus there is a need to account for intraparticle and external mass transfer limitations[34,35]. It is assumed that due to limited penetration of reactants through the char, the combustion reaction acts on the surface and therefore decreases both the mass and size of the particle without significantly affecting its density. This is also known as the shrinking unreacted particle model (SUPM)[9] of char combustion where the ash layer is assumed to detach from the surface. Even though the fines are much more reactive compared to the mother particles due to their smaller size, it can be assumed that they do not further react with oxygen once they are generated because of their short residence time. This is valid based on the conditions considered in the time-scale analysis, but in practice will strongly depend on the availability of oxygen in the freeboard. In both combustion and gasification cases, intraparticle temperature gradients are neglected[21], and the heat transfer from the bed material to the active particles is sufficiently fast that no temperature difference exists between the particle surface and the boundary layer.

The mathematical model consists of a system of coupled ordinary differential equations (ODE's) describing a batch-wise conversion of mother char particles. An initial charge of mother particles formed by devolatilization and primary fragmentation of average initial

diameter $d_{ch,0}$ in m, initial density, $\rho_{ch,0}$ in kg/m^3 and initial mass $m_{ch,0}$ in kg, so that the initial number of particles $n_{ch,0}$ can be computed,

$$n_{ch,0} = 6m_{ch,0}/(\pi d_{ch,0}^3 \rho_{ch,0}) \quad (5)$$

Unlike coal char particles which can be represented by spherical geometries, biomass particles can have irregular shapes, so the average char diameter used throughout this paper refers to the volume/surface mean diameter- the diameter of a sphere with equivalent volume to surface area ratio as the particle. Subsequently, through the additional specification of particle aspect ratio and shape, it is possible to describe pellet (cylindrical) or flake/slab shaped particle geometries[29]. See the Appendix for these definitions.

In this transient batch system, the carbonaceous portion of char particles is consumed by gasification, combustion, and attrition,

$$dm_{ch}/dt = -(R_{gasif} + R_{att} + R_{comb})m_{ch} \quad (6)$$

where sections 2.1 and 2.2 and 2.3 discuss in detail how the attrition, gasification, and combustion rates $R_{att}, R_{gasif}, R_{comb}$, respectively, with units of 1/s are evaluated and m_{ch} is the mass of the carbonaceous (ash-free) portion of the particle. Because ash is assumed to detach from the particle during combustion, the ash fraction of the char is consumed by attrition and combustion on the surface:

$$dm_{ash}/dt = -(R_{att} + R_{comb})m_{ash} \quad (7)$$

Meanwhile, gasification reactions diminish the density of the char,

$$d\rho_{ch}/dt = -R_{gasif}\,\rho_{ch} \quad (8)$$

It is also useful to define non-dimensional char conversion parameters,

$$X_\rho = (\rho_{ch,0} - \rho_{ch})/\rho_{ch,0} \quad (9)$$

$$X_m = (m_{ch,0} - m_{ch})/m_{ch,0} \quad (10)$$

$$X_g = X_m - m_{att}/m_{ch,0} \quad (11)$$

The first (X_ρ) refers to the extent to which the mother char particles have undergone gasification, the second (X_m) refers to the extent that char has been converted by all pathways (gasification combustion or, attrition), while (X_g) refers to the mass fraction of the initial char gasified or combusted. Assuming the mother particles remain spherical and their number, $n_{ch,}$ remains constant until they are completely converted, the average diameter of the char particles, d_{ch} in m, can be computed by combining equations (5) and (9) and (10),

$$d_{ch} = \left(\frac{6}{\pi}\frac{m_{ch}}{n_{ch}\rho_{ch}}\right)^{1/3} = d_{ch,0}\left(\frac{1 - X_m}{1 - X_\rho}\right)^{1/3} \quad (12)$$

According to our modeling assumptions and Equation (12), a batch of char particles converted solely through gasification exhibits a constant average char diameter (since $X_m = X_\rho$ under these conditions), while the average density would eventually diminish to 0 while X_ρ reaches 1. Meanwhile, a batch of char particles converted solely through attrition or combustion, would experience a constant char density (since $X_\rho = 0$ under these condition), while the average char diameter would eventually shrink to 0. The ability of this model to represent any combination of these processes in parallel is particularly crucial for representing the gasification-assisted attrition phenomenon in which variation in char density and size occur simultaneously.

If secondary fragmentation of the mother particles occurs, then the number of char particles is not constant during conversion, and the average char diameter can be modified by a secondary char multiplication factor $n_{2,}$

$$d_{ch} = d_{ch,0}\left(\frac{1-X_m}{1-X_\rho}\frac{1}{n_2}\right)^{1/3} \quad (13)$$

For the fluidized bed gasification of lignite char[15], n_2 has previously been written as a function of the carbon conversion,

$$n_2 = 1 + (n_{2m} - 1)\left(\frac{X_g - X_g^*}{1 - X_g^*}\right) \quad (14)$$

Where the two empirically determined parameters are n_{2m}, the maximum number of fragments generated and X_g^*, the threshold level of conversion beyond which fragmentation begins to occur. Because of the lack of necessary parameters for n_2 under biomass char gasification/combustion conditions, secondary fragmentation is neglected (i.e. $n_2 = 1$) in the current study but could be included when such data exists. The sensitivity of secondary fragmentation under combustion is commented on in later sections. The following sections describe in detail how to evaluate the rates of attrition, gasification, and combustion rate expressions.

2.1.Fragmentation, attrition, and elutriation modeling

When raw fuel particles are introduced into a reactor they rapidly undergo devolatilization and primary fragmentation resulting in a distribution of mother char particles of smaller size. Scala et al. [33] give a simplified model to predict an initial average char diameter $d_{ch,0}$ from an initial raw particle diameter $d_{f,0}$ in m,

$$d_{ch,0} = d_{f,0}/(\varphi_s n_1)^{1/3} \quad (15)$$

where φ_s, and n_1, are the shrinkage and primary fragmentation factors, respectively. The primary fragmentation factor, n_1 refers to the total number of fragments generated by a single biomass particle. For a given feedstock, it has shown dependence on the initial particle size, with larger particles generating more fragments than smaller ones[33]. Because the penetration of reactants into the particle during the devolatilization process is limited, these factors are not strongly dependent on the gas phase environment of the bed[36]. Due to a lack of available data under gasification conditions, the secondary fragmentation of these mother char particles during their lifetime is neglected.

The attrition rate of mother char particles, R_{att} (1/s) is modeled as in Ref.[5,20,33]:

$$R_{att} = K_{att,0}\left(u_0 - u_{mf}\right)/d_{ch} \cdot F_{att} \tag{16}$$

where $K_{att,0}$ is a dimensionless attrition constant ranging from 10^{-7} to 10^{-8} for various carbonaceous feedstocks[5], u_{mf} is the minimum fluidization velocity of the bed material in m/s, and F_{att} is our proposed dimensionless structural attrition profile,

$$F_{att}\left(X_\rho\right) = \left(1 - X_\rho\right)^{-q} = \left(\rho_{ch}/\rho_{ch,0}\right)^{-q} \tag{17}$$

where q is a structural attrition parameter that requires fitting. The purpose of this profile is to reflect the effects of gasification-assisted attrition. As noted by Basu and Subbarao[37], in comparing coal, petroleum coke, and electrode carbon, the attrition constant $K_{att,0}$ in equation (16) was a strong function of the hardness and shape of the particles. Since hardness itself is not measured or modeled, the density is subsequently used as a proxy variable. The form of this proposed profile suggests that the attrition rate should experience a hyperbolic increase as the hardness (and density) of the char decreases.

2.2.Char gasification reactivity modeling

The reactivity of char R_j (j=CO_2 H_2O, or O_2), has units of (1/sec) and is defined as the conversion rate per unit mass remaining,

$$R_j = -\frac{1}{m_{ch}}\frac{dm_{ch}}{dt} = r_j \cdot F_j\left(X_\rho\right) \tag{18}$$

The reactivity of chars is usually separated into a chemical kinetics rate, r_j, and a dimensionless structural profile $F_j(X_\rho)$ which represents a normalized surface area and/or concentration of active sites for heterogeneous reactions. The structural profile is usually assumed to be invariant over the range of temperature and pressures used in the fitting[38]; although care should be taken during extrapolation outside the fitting domain[39]. In some cases, the chemical kinetics rate is fitted at a representative degree of conversion, X_{fit}, where $F_j(X_{fit})$ is equal to unity[38,40]. In other cases, the kinetics rate is averaged over a certain range of conversion[17].

The most common approach to modeling the chemical kinetics rate, r_j in pure gasifying agents is a power-law model as shown in equations (19) and (20) in Table 3**.** These models should be avoided when significant partial pressures of carbon monoxide or hydrogen are present (0.1-0.3 bar) as these have strong inhibitory effects[10,41]. A more general and robust approach are the LH kinetics expressions shown in equations (22) and (21) in the same table, which have been fitted for birch chars at atmospheric partial pressures of steam (<1bara). During the experiments used to derive these expressions, Kramb et al. rapidly heated (~20°C/s)[42] the char sample in the TGA, and no cooling occurred between the devolatilization stage and the gasification, thus these chars more closely simulate the actual conditions in a fluidized bed gasifier. Still, extrapolation of these kinetics at the elevated operating pressures of industrial gasifiers (>30bara) is quite

uncertain, but to our knowledge, these are the most up to date LH-type kinetics parameters available for biomass chars and are employed throughout this study.

Because of the complex catalytic nature of the ash-forming components in biomass, there is- as yet- no accepted way to describe the structural profile, $F_j(X)$ in biomass chars. This is an area of ongoing investigation[11,19]. The uniform conversion model is assumed as in previous works[5,41] where $F_j(X)$ is taken as invariant with conversion; although an arbitrarily complex function could be applied in the context of this numerically integrated model.

Table 3. Chemical kinetics rates for gasification reactions

Source	Fuel	Kinetic rate expression (1/s)	Eq	Range of applicability
Guizani et al., 2013 [40]	Beech	$r_{CO_2} = k_{CO_2} p_{CO_2}^{0.55}$ $k_{CO_2} = 5.518 * 10^4 \exp(-154{,}000/R_g T)$	(19)	$1123 < T < 1273\ K$ $0.1 < p_{CO_2} < 0.3\ bar$
Guizani et al., 2013 [41]	Beech	$r_{H_2O} = k_{H_2O} p_{H_2O}^{0.64}$ $k_{H_2O} = 2.63 * 10^4 \exp(-139{,}000/R_g T)$	(20)	$1023 < T < 1223\ K$ $0.1 < p_{H_2O} < 0.3\ bar$
Kramb et al., 2014[19]	Pine	$r_{CO_2} = \frac{k_{CO_2} p_{CO_2}}{1 + \kappa_{CO_2} p_{CO_2} + \kappa_{CO} p_{CO}}$ $k_{CO_2} = 5.94 * 10^7 \exp(-180{,}000/R_g T)$ $\kappa_{CO_2} = 4.64 * 10^{-1} \exp(45{,}000/R_g T)$ $\kappa_{CO} = 4.296 * 10^{-9} \exp(213{,}000/R_g T)$	(21)	$1023 < T < 1123\ K$ $0.8 < p_{CO_2} < 1\ bar$ $0 < p_{CO} < 0.2\ bar$
Kramb et al., 2014[19]	Pine	$r_{H_2O} = \frac{k_{H_2O} p_{H_2O}}{1 + \kappa_{H_2O} p_{H_2O} + \kappa_{H_2} p_{H_2}}$ $k_{H_2O} = 6.3854 * 10^5 \exp(-153{,}823/R_g T)$ $\kappa_{H_2O} = 1.3032 * 10^{-2} \exp(59{,}199/R_g T)$ $\kappa_{H_2} = 1.58431 * 10^{-3} \exp(104{,}725/R_g T)$	(22)	$1023 < T < 1123\ K$ $0.86 < p_{H_2O} < 1\ bar$ $0 < p_{H_2} < 0.14\ bar$
R_g is the universal gas constant in J mol^{-1} $K^{-1,}$ and T is temperature in K, and p is partial pressure in bara.				

Then, the gasification rate (1/s) to be used in equation (6) is the sum of all heterogeneous rates, which can be adjusted by a fitting parameter, psi ψ,

$$R_{gasif} = \psi(r_{CO_2} F_{CO_2} + r_{H_2O} F_{H_2O}) \quad (23)$$

2.3.Combustion rate

Due to the high reactivity of biomass chars, the overall combustion rate must incorporate kinetic as well as internal and external diffusion limitations. Char combustion models can be classified

as dependent on apparent or intrinsic kinetics[43]. When the latter is adopted, the particle reaction rate depends on intrinsic reactivity, pore surface area, the concentration (or mass density) of carbon in the char, and the effective diffusivity of reactants through the porous char matrix. Meanwhile, the apparent kinetics approach lumps internal diffusion and chemical kinetics into a single *burning rate*- also called *surface reaction rate* (usually with units of m/s) written with an Arrhenius type expression[44,45]. Many models for biomass combustion[45,46] sources cite coal-specific sources for the burning rate[47,48]. It is usually argued[29] that under certain particle size and reactive conditions, biomass combustion is largely controlled by external mass transfer limitations so that this assumption introduces negligible error. However, this has been shown in the time scale analysis in Table 1 to be invalid for millimeter scale biomass chars[35]. In the interest of developing a rigorous model of biomass combustion that is relevant for arbitrarily sized char particles and feedstocks, it is clear the intrinsic approach is necessary. Thus, the method is to represent an effective combustion rate R_{comb} [1/s] in equation (6) as a single expression incorporating the three limiting processes,

$$R_{comb} = R_{O_2}\eta_{int}\eta_{ext} \tag{24}$$

where R_{O_2} is the combustion reactivity under kinetically-limited conditions, η_{int} is the internal effectiveness factor, and η_{ext},is the external effectiveness factor. The following section defines the necessary inputs to each contribution and derivation of this expression is provided in the Appendix. A burning rate that properly accounts for the physical properties of biomass chars is also rigorously derived in the Appendix, which can be used in future modeling studies.

2.3.1. Combustion kinetics

The reactivity of biomass char to oxygen, R_{O_2} [1/s] has been adapted from the work of Di Blasi et al., 1999[49] for pine sawdust and can also be separated into a kinetic rate, r_{O_2} with units of 1/s and a dimensionless structural profile, F_{O_2},

$$R_{O_2} = r_{O_2} F_{O_2} \tag{25}$$

where the kinetics exhibits a first-order dependence on the concentration of oxygen, C_{O_2} in $mol_{O2}/m^3/s$,

$$r_{O_2} = k_{O_2} C_{O_2} \tag{26}$$

k_{O_2} has units of $m^3/mol_{O2}/sec$,

$$k_{O_2} = 1.5 * 10^6 \exp\left(-\frac{13{,}078}{T}\right) \frac{R_g T}{101325} \tag{27}$$

R_g is the ideal gas constant in J/mol/K, T is the particle temperature in K, and the structural profile,

$$F_{O_2} = \left(1 - X_\rho\right)^{1.2} \tag{28}$$

suggests that the reactivity decreases in an approximately linear fashion as the conversion proceeds.

2.3.2. Estimation of internal diffusion transport limitations

A major challenge in this approach is the estimation of the transport properties given the complex pore structure of the coal and biomass chars[50], which depend strongly on feedstock and the conditions under which they were generated. The internal diffusion limitations are governed by the structural properties which include the concentration of carbon C_c in mol_C/m^3, char void

fraction, $\varepsilon_{g,ch}$, and the effective diffusivity of the reactant (oxygen) through the porous char matrix. Unfortunately, most of these properties are not commonly measured or explicitly reported, thus what follows is a method of estimating these properties from more commonly measured values for biomass pine wood chips (PWC) and spruce wood pellets (SWP). The necessary data inputs and computed properties of these two feedstocks are summarized in Table 4. Note that the same methodology could be applied to other feedstocks where the input data was available.

Char particles are assumed to be composed entirely of carbon, ash, and void.

$$\varepsilon_g = 1 - \varepsilon_{ch} - \varepsilon_{ash} \quad (29)$$

All hydrogen and oxygen contained in the biomass is assumed to be released during devolatilization. The solid volume fractions ε_j (units of $m^3_j/m^3_{particle}$) can be inferred from their apparent densities ρ_j and skeletal densities $\rho_{wall,j}$. The skeletal densities of biomass, carbon, and ash, are not assumed to depend on feedstock.

$$\varepsilon_{bio} = \rho_{bio} / \rho_{wall,bio} \quad (30)$$

$$\varepsilon_{ch} = \rho_{ch} / \rho_{wall,ch} \quad (31)$$

$$\varepsilon_{ash} = \rho_{ash} / \rho_{wall,ash} \quad (32)$$

The char yield, Y_{ch} (kg_{ch}/kg_{bio}) produced from biomass devolatilization is not usually measured directly, so as a reasonable estimate, it can be assumed to be the same as the fixed carbon content of the original biomass. It can also be reasonably assumed that all the ash in the original biomass is retained in the char. With these assumptions, the initial apparent carbon density (kg_{carbon}/m^3_{char}) and apparent ash density (kg_{ash}/m^3_{char}), can be computed,

$$\rho_{ch,0} = \rho_{bio} Y_{ch} \varphi_s \quad (33)$$

$$\rho_{ash,0} = \rho_{bio} Y_{ash} \varphi_s \quad (34)$$

where, φ_s($m^3_{particle,biomass}/m^3_{particle,char}$) has been defined previously in the literature[32,33] as a feedstock-dependent, dimensionless shrinkage parameter, and Y_{ash} is the ash content of the biomass in ($kg_{ash}/kg_{biomass}$). The molar concentration of carbon is,

$$C_c = \rho_{ch}/MW_c \quad (35)$$

where MW_c is the atomic weight of carbon in kg_C/mol. As shown in Table 4, the initial carbon concentrations are very different for PWC and SWP (10,200 versus 24,300 mol_C/m^3) with the latter closer to that of sewage sludge char (33,900 mol_C/m^3) as reported in Dennis and Hayhurst[51]. This is expected since the latter is a much more dense material to begin with. The estimated initial void fractions are 0.935 for PWC and 0.85 for SWP. Note that although a significant amount of volumetric shrinkage occurs[32,33] during devolatilization; the large majority of the carbon present in the original biomass is contained in the volatiles, thus the resultant chars tend to be *more* porous than their raw biomass particles.

Diffusion through the char is often described by Fick's law modified with an effective diffusion coefficient[38]. The binary diffusivity of oxygen D_{binary} (units of m^2/sec) in air is well fitted by the following correlation shown in Table 4. However, the diffusion within the char is reduced due to constrictions and the nonlinear path the molecules must travel. An effective diffusion coefficient which takes this into account is often introduced[52,53],

$$D_{eff} = D_{binary}\left(\varepsilon_g \sigma/\tau_p\right) \quad (36)$$

where σ is the dimensionless constriction factor and τ_p is the tortuosity. While a range of values for these two parameters have been assumed in coal and biomass char kinetics literature[54] as generally ranging between ($0.01 < \varepsilon_g\sigma/\tau_p < 0.1$)[53] or $\sigma/\tau_p = 6$[50], it was found that $\sigma/\tau_p = 0.2\varepsilon_g^3$ fit the data from Prins and Van Swaaij[55] – a study which actually measured the effective diffusivity versus porosity in coal chars. For a typical reactor condition of 800°C and 1atm of

pressure, the resulting conversion averaged-effective diffusivities are $3.25*10^{-5}$ and for PWC and $2.6*10^{-5}$ m^2/sec for SWP due to its lower void fraction (higher apparent char density).

The internal effectiveness factor for a spherically equivalent geometry can be defined as the actual reaction rate divided by the rate if a uniform reactant concentration existed across the particle[56],

$$\eta_{int} = \left(\frac{1}{\tanh(3\phi)} - \frac{1}{3\phi}\right) \quad (37)$$

Where the Thiele modulus, ϕ is defined as,

$$\phi = \frac{d_{ch}}{6}\sqrt{\frac{k_{O_2} C_c \lambda}{D_{eff}}} \quad (38)$$

and the stoichiometric coefficient, λ is defined (mol_{O2}/mol_C). For the full derivation of this expression see the Appendix. While the above approach is shown to estimate the initial properties of the char, it is similarly applied to compute the properties of the char while it is undergoing simultaneous changes in density and size. As a result the internal/external combustion effectiveness factors employed in equation (24) vary throughout the conversion of the char particle.

2.3.3. Estimation of external transport limitations

The transport of oxygen from the bulk through the boundary layer to the particle surface is a significant limitation during the combustion of millimeter size biomass char particles[9,24,51,55].

The mass transfer coefficient (in m/s) depends on the Sherwood number for the particle as well as the diffusivity of oxygen in the boundary layer,

$$h_m = ShD_{binary} / d_{ch} \quad (39)$$

Due to the sensitivity of the combustion rate to external mass transfer limitations, some studies use corrective[24] or limiting factors[57] for the mass transfer coefficient. One reason is that the well-

known Ranz-Marshall correlation (valid for 20<Re<2000[58]) is often misapplied in fluidized bed and fixed bed applications where the Reynolds number of the particle (defined in Table 4) is significantly lower (Re<10). The correlation published in Scala, 2007[59] is shown in Table 4 and was developed specifically for reacting spherical particles under fluidized bed conditions at elevated temperatures (723K) and atmospheric pressure and fitted their experimental data within ±10%. The external effectiveness factor is defined here as,

$$\eta_{ext} = \frac{1}{\eta_{int}\phi_{ext} + 1} \quad (40)$$

Where the external Thiele modulus, ϕ_{ext} is also defined here as,

$$\phi_{ext} = \frac{d_{ch} k_{O_2} C_c \lambda}{6 h_m} \quad (42)$$

Table 4. Relevant transport properties for computing transport-related combustion properties of pine wood chip *pinus radiata* char (PWC) and spruce wood pellet (SWP) char

Property	**Correlation or value**	**Source**
Char structural properties		
Biomass skeletal (wall) density	$\rho_{wall,bio} = 1500$ kg/m^3	Ragland et al. 1991[60]
Char skeletal (wall) density	$\rho_{wall,ch} = 1888$ kg/m^3	Inferred from Chirone et al., 2008[32]
Ash skeletal density	$\rho_{wall,ash} = 2600$ kg/m^3	(Assumed to be silicon dioxide)
Apparent biomass particle density	$\rho_{bio} = 550$ kg/m^3 (*PWC*) $\rho_{bio} = 1300$ kg/m^3 (*SWP*)	Scala et al., 2006[33] Scala et al., 2006[33]
Char yield (fixed carbon on a dry basis)	$Y_{ch} = 0.133$ kg$_{char}$/kg$_{biomass}$ (*PWC*) $Y_{ch} = 0.171$ kg$_{char}$/kg$_{biomass}$ (*SWP*)	Ammendola 2013[14] Ammendola 2013[14]
Ash content/yield (Proximate analysis dry basis)	$Y_{ash} = 0.00307$ kg$_{ash}$/kg$_{biomass}$ (*PWC*) $Y_{ash} = 0.00327$ kg$_{ash}$/kg$_{biomass}$ (*SWP*)	Ammendola 2013[14] Ammendola 2013[14]
Devolatilization shrinkage factor	$\varphi_s = 1.68\ m^3_{biomass}/m^3_{char}$ (*PWC*) $\varphi_s = 1.31\ m^3_{biomass}/m^3_{char}$ (*SWP*)	Ammendola 2013[14] Ammendola 2013[14]
Initial char void fraction	$\varepsilon_{g,0} = 0.935$ (*PWC*) $\varepsilon_{g,0} = 0.845$ (*SWP*)	Eqn. (29)
Initial char carbon concentration	$C_{c,0} = 10{,}232$ mol$_C$/m^3 (*PWC*) $C_{c,0} = 24{,}273$ mol$_C$/m^3 (*SWP*)	Eqn. (26)
Mass transfer properties		
Binary diffusivity	$D_{binary} = 1.5815 * 10^{-4} \left(\frac{T}{1000}\right)^{1.75} \frac{101325}{P}$ (m^2/sec)	(Binary diffusion coefficient for oxygen in air)
Effective diffusivity	$D_{eff} = D_{binary}\ 0.2\varepsilon_g^3$ (m^2/sec)	Fitted to data from Prins and Van Swaij, 1986[55]
Dynamic viscosity	$\mu_f = 1.98 * 10^{-5} \left(\frac{T}{300}\right)^{\frac{2}{3}}$ (Pa-s)	Purnomo et al, 1990[61]
Sherwood number	$Sh = 2\varepsilon_{mf} + 0.7\left(Re_p/\varepsilon_{mf}\right)^{1/2} Sc^{1/3}$	Scala, 2007[59]
Reynolds number	$Re_p = \rho_f u_{mf} d_{ch}/\mu_f$	
Schmidt number	$Sc = \mu_f/(\rho_f D_{binary})$	

Voidage at minimum fluidization	$\varepsilon_{mf} = (14\Psi)^{-1/3}$ Ψ =0.9 (Silica sand)	Wen and Yu, 1966[62]

2.4.Numerical solution

To summarize, a *transient* model has been developed to predict the behavior of a batch input of particles gasified or combusted under a specified time, temperature, pressure, and reactive conditions: the transient particle model is a system of ODE's requiring initial char conditions (size, density, etc.) and reactor specifications (size, temperature, pressure, and gas phase concentrations). The ODE's are integrated in MATLAB using ode15s for specified time or until the mass of char remaining in the reactor is 0. Through a residence time-based averaging presented later in Section 3.3, the transient model results can be used to predict steady state statistics for a continuously-fed system.

3. **Results and Discussion**

In section (3.1), the transient model is applied to fit attrition kinetics parameters from the experimental gasification data published by Ammendola et al.,[14]. The fitted parameters are used to validate the batch transient model predictions under combustion conditions in the section 3.2. Then in section 3.3 a residence time based averaging method is presented in order to predict steady-state statistics (bed inventory, char conversion) for continuously fed systems. Using this methodology, a hypothetical continuously fed steam/CO_2 blown gasifier is simulated to study the impact of temperature, pressure, and other input/fitted parameters on steady state char conversion and bed inventory. Lastly, the model limitations and areas for future work are highlighted in section 3.4.

3.1. Transient char CO_2 gasification of SWP and PWC chars

In the study by Ammendola et al.[14] batch char gasification experiments were performed under CO_2/N_2 atmospheres to elucidate the phenomenon of gasification-assisted attrition. Spruce pellets and pine wood chips were initially fed into a fluidized bed reactor under inert conditions (100% N_2) at 800 $^{\circ}$C until devolatilization and primary fragmentation was finished (5min) and the resultant chars were retrieved for particle size analysis. In the second part of the experiment, batch quantities (2 gram charges) of previously devolatilized char were fed into a fluidized bed under gasification conditions (see Table 5). During this time, elutriated fines were collected in various filters with both their weight and operating time interval recorded, while carbon conversion (X_g) was tracked by integrating outlet gas (CO_2/CO) concentrations. In a previous study by the same authors, it was indicated that the elutriation rate could be measured within ±10% accuracy[33].

In our study, three dimensionless model parameters- the initial attrition constant $K_{att,0,}$ a reactivity factor ψ, and the structural attrition profile constant, $q,$ were fitted against the available outputs. The three parameters are fitted as an inverse problem by minimizing the sum of the squared residuals between the predicted/actual carbon conversion profile and elutriation rates. These fitted parameters are summarized in Table 5. The aspect ratio of the spruce wood pellet (SWP) chars was assumed to be the same as the raw pellets[33]. The detailed geometry of the wood chips were not explicitly reported in Ammendola's study[14]; however, they were reported as having a highly irregular but paralleliped geometry[33] in Scala's study. Lacking additional details, they were approximated as a flake with an aspect ratio of 2 in this study.

Table 5. Experimental conditions for the gasification/combustion and attrition study by Ammendola et al. 2013[14] and Scala et al. 2006[33]. Fitted parameters from this study.

Reactor properties	**Value**	
Bed material size, density, mass: $d_{p,}\rho_{p,}m_{bed}$	350 μm, 2600 kg/m^3, 0.18 kg	
Fluidization, superficial velocity: $u_{mf,}u_0$	0.0438, 0.8 m/s	
Bed temperature, bed diameter $T_{bed,}$ d_{bed}	800 °C, 0.04 m (Ammendola al. 2013) 850 °C, 0.04 m (Scala et al., 2006)	
Inlet gas composition, *Gasification conditions* *Combustion conditions*	 60% CO_2 (%vol),40% N_2 (%vol) 4.5% O_2 (%vol) 95.5 (%vol)	
Initial char loading, $m_{ch,0}$	2 grams	
Feedstock properties		
Feedstock	Spruce wood pellet char (SWP)	Pine wood chip char (PWC)
Initial biomass diameter, $d_{f,0}$	$d_{f,cyl,0}$=6 mm	$d_{f,slb,0}$=10.4 mm
Reported mean diameter, $d_{ch,0}$	$d_{ch,cyl,0}$=4.9 mm	$d_{ch,slb,0}$=5.3 mm
Reported fragmentation factor, n_1	1.4	4.5
Particle geometry	Cylinder	Flake
Aspect ratio	$AR_{cyl} = 20/6$ (reported)	$AR_{slb} = 2$ (assumed)
Char reactivity	Eqn (9)	Eqn (15)
Fitted parameters (this study)		
Initial attrition constant $K_{att,0} \cdot 10^{-7}$	0.8	5.5
Gasification reactivity factor, ψ	0.184	0.24
Attrition structural profile constant, q	2.5	2

Figure 2a exhibits the fitted model results for elutriation rate (kg/min) versus time (min) for the spruce wood pellet (SWP) char gasification which demonstrate a drastic increase then decrease in elutriation rate over the course of conversion. There are two ways that the model- specifically equation (16)- reflects the apparent increase in elutriation rate: first, there is the added structural attrition term which accounts for the reduction in hardness as the density of the char decreases, and secondly the particle diameter decreases drastically especially towards the end of conversion increasing its surface area to volume ratio (as shown in Figure 4). The decrease in elutriation rate after 100 minutes is associated with the reduced inventory of char remaining in the gasifier. Figure 2b shows that the fitted model results match very well with the output of greatest significance- the cumulative fraction of char attrited/elutriated was 30%wt of the original mass.

The fitted parameters demonstrate that wood chip char demonstrates ~7 times larger initial attrition constant compared to spruce pellets reflecting their reduced initial hardness. These results are expected given that pelletization imparts increased density and therefore hardness to the original feedstock, some of these mechanical effects are still apparent in the resultant devolatilized chars.

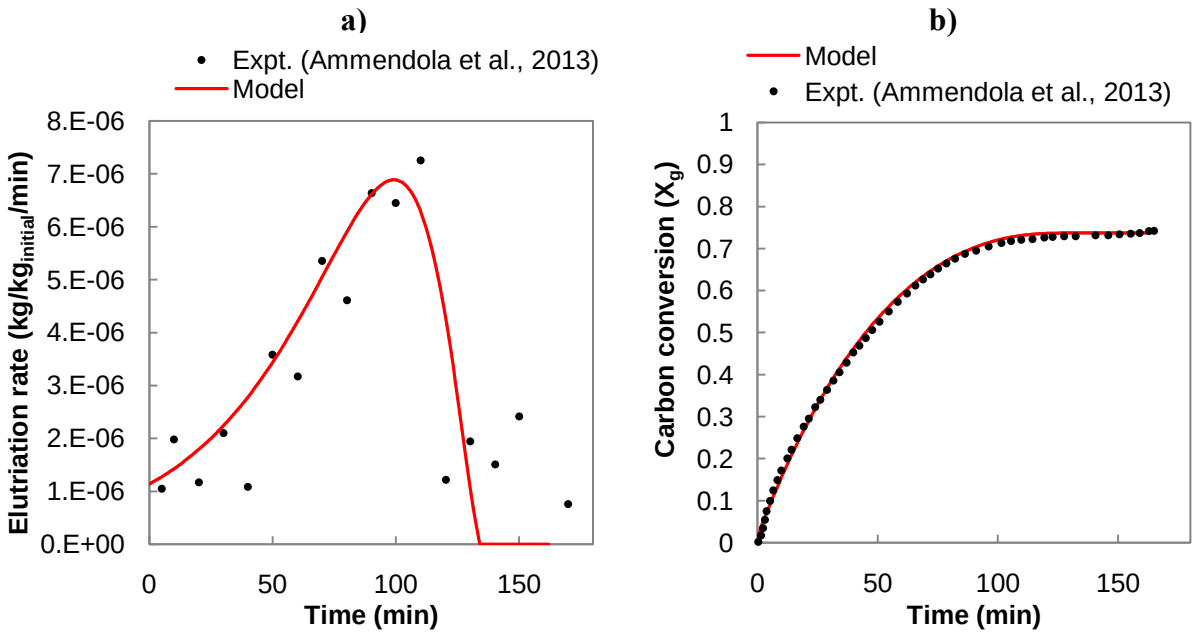

Figure 2a,b.- Elutriation rate (kg/kg$_{initial}$/min) versus time (a) and carbon conversion (X_g) versus time in minutes for spruce wood pellet char gasification (b).

Figure 3a and b show the fitted model results against the experimental elutriation and conversion data, respectively, for the pine wood chip (PWC) char gasification experiments. The experimental results demonstrate a rapid increase then decrease in absolute attrition rate (kg/min) peaking at 15 minutes. The model meanwhile shows a much later (38 min) and broader peak in attrition rate. A possible explanation for this discrepancy is the shape of the particles. In the model, the char particles are assumed to be maintain their original geometry during conversion;

however in reality, the initially rough and irregular edges of freshly formed char from wood chips may initially be more susceptible to attrition- explaining the much earlier peak in attrition observed in the experiment. In order to represent this, more information on the evolution in char shape during conversion would be needed. Nevertheless, the overall profile of char conversion is represented well, and the model predicts that 50.9% of the initial char is converted by gasification agreeing with the experimentally measured value of 51.6%wt.

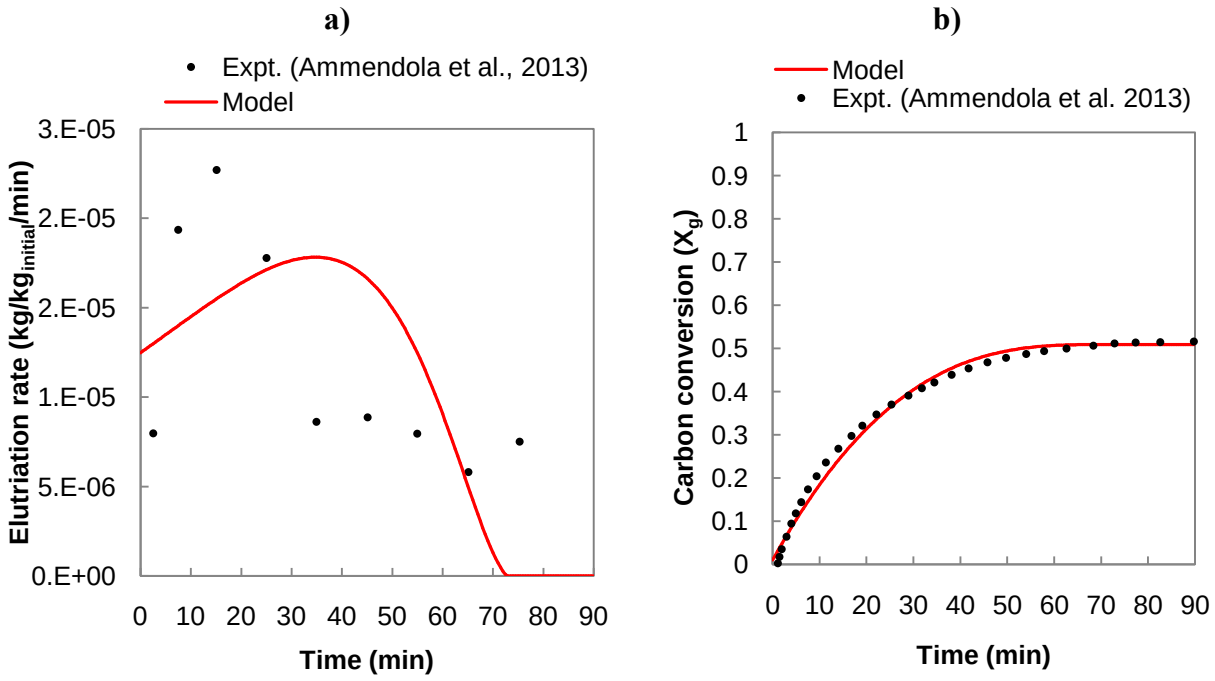

Figure 3a,b- Elutriation rate (kg/kg$_{initial}$/min) versus time (a) and carbon conversion (Xg) versus time in minutes for pine wood chip char gasification (b).

Figure 4a,b shows the model predictions for normalized char diameter and density versus char conversion for the two different feedstocks under gasification conditions. The char diameter demonstrates a unique behavior only explained by the gasification assisted attrition mechanism. The model describes both the reduction in density (see Figure 4b) - caused by gasification- and

size caused by attrition. As a result, at early stages of conversion, the attrition rate is relatively low because the char's structure is still intact. However, as the density and hardness of the char decreases the attrition rate accelerates non-linearly. This acceleration in the reduction of diameter could be interpreted as a disintegration of the char to a miniscule size, at which point the gasifier rapidly becomes empty of char and conversion reaches an asymptote. The predictions show that due to rapid attrition, the diameter of the char reaches 0 before the average density of the char reaches 0.

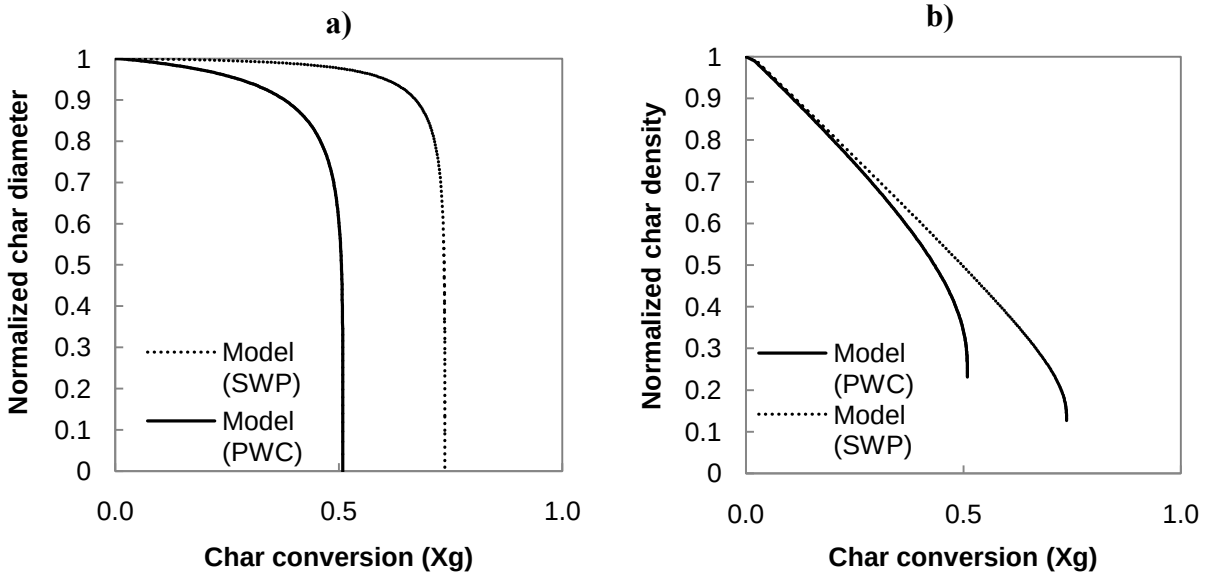

Figure 4a,b- Model predictions for normalized char diameter $d_{ch}/d_{ch,0}$ (a) and normalized char density versus $\rho_{ch}/\rho_{ch,0}$ (b) char conversion (X_g) for SWP and PWC gasification

3.2. Transient char combustion of SWP and PWC chars

In the same study by Ammendola et al.[14] batch char combustion/attrition experiments were also performed in a 4.5 vol% oxygen, 95.5% vol nitrogen environment in order to identify the impact of feedstock on combustion efficiency. The reactive conditions are summarized in Table 5. The

previously-fitted attrition related parameters were not modified in the model. The only changes to the model were the relevant input reactive conditions. However, in the following comparisons, the sensitivity of the combustion model to the assumption of the number of particle fragments generated during devolatilization (n_1 from equation (15) is evaluated. A strong sensitivity of burnout time to the fragmentation factor is expected since it governs the initial char particle size, where the burnout time, $t_{burnout}$, is defined here as the time at which conversion (X_g) reaches 99% of its asymptotic value. The original experiment found that spruce pellets generated an average of 1.4 char fragments while pine wood chips created 4.5. However, no standard deviation or variability was given for this parameter which could be expected to be significant. Further, it is reasonable to hypothesize that the act of cooling down, retrieving, and sieving the fragile char particles for analysis might actually cause further fragmentation than under the actual conditions. If true, then the reported fragmentation factors could be considered an upper bound.

Figure 5 and Figure 6 show the elutriation rate and carbon conversion profile for the SWP and PWC chars, respectively. The predicted final carbon conversion achieved during SWP combustion matches extremely well with the experimentally measured value of 99.7%, regardless of which fragmentation factor is assumed. Assuming n_1=1 and 1.4, the model predicts a burnout time of 17 minutes and 14 minutes, respectively. Overall the former agrees better with the burnout time experimental data ($t_{burnout}$=20 minutes). The attrition profile is only slightly affected by the fragmentation factor, and the integrated amount of attrited mass is relatively similar. Overall, the combustion conditions result in very different attrition behavior than under the gasification conditions. Attrition is monotonically decreasing throughout conversion during combustion because the total mass of particles remaining in the reactor decreases more rapidly than their average diameter. The limited penetration of reactants into the char particle means that

the overall hardness/density of the particle is constant during conversion, thus avoiding the gasification-assisted attrition phenomenon.

The experiment reported that PWC char combustion occurred in ~3.4 minutes- almost 6 times faster than the SWP combustion (~20 minutes). This is explained by the much higher carbon concentration in the pellet-derived char compared to the chip. Additionally, the volume/surface mean diameter of the pellets is larger than the chips, and because of the external and internal mass transfer limitations, a larger size results in longer burnout times. Figure 6 shows that the model is able to account for these differences in feedstock accurately and predicts a PWC burnout time between 3.3 and 4 minutes for n1=4.5 and 3, respectively. A final carbon conversion of 99% is predicted by the model using either fragmentation factor, which is higher than the experimentally reported conversion of 97.35%. This is also reflected by the significant under-prediction in the attrition rate by the model results. It is possible that the high observed attrition rate caused by the grinding of particle irregularities (i.e. edges and corners) could explain some of the discrepancy; however, the consistently higher attrition rate suggests that the PWC combustion exhibits enhanced attrition compared to gasification conditions. Given that this difference of 1.5%wt corresponds to a discrepancy of only 0.03grams of elutriated char, it is unclear whether this is within the absolute precision of the experimental method. As a result, further validation is made against additional PWC char combustion data from the literature.

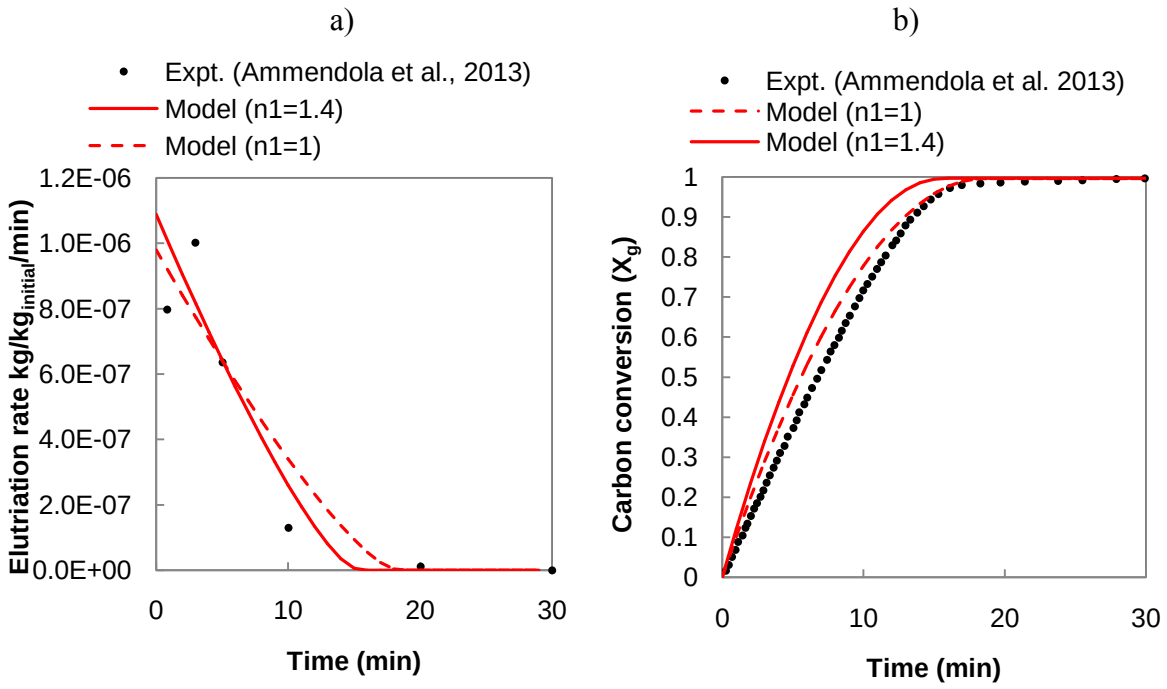

Figure 5a,b- Elutriation rate (kg/kg$_{initial}$/min) versus time (a) and carbon conversion (X_g) versus time in minutes for spruce wood pellet (SWP) char combustion (b).

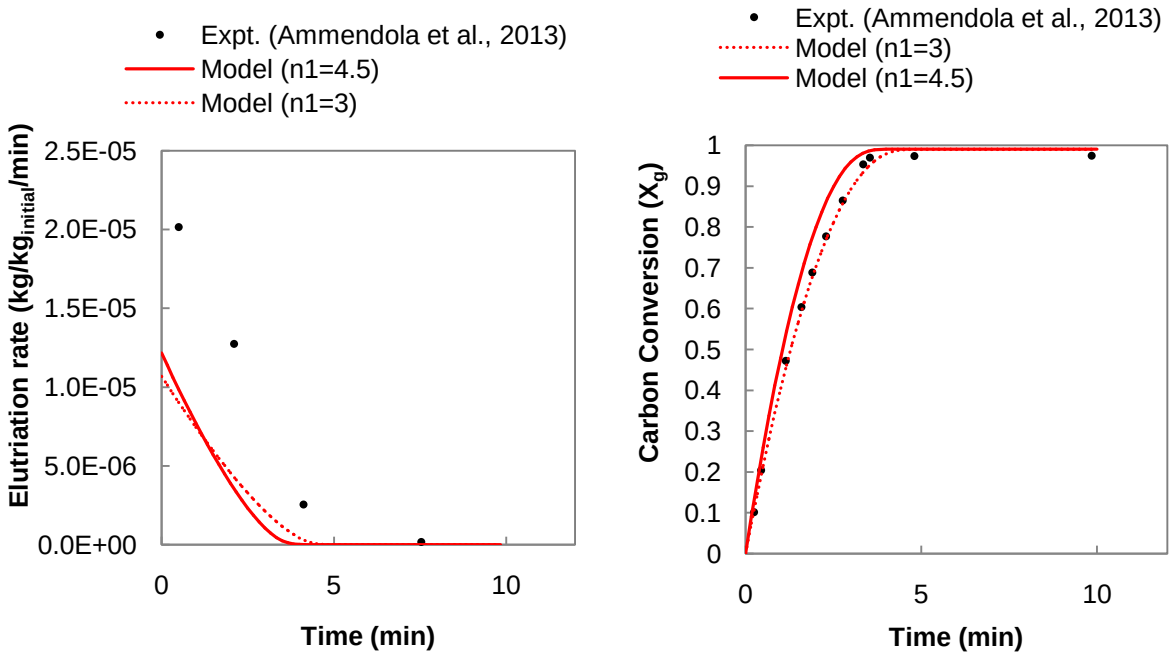

Figure 6a,b Elutriation rate versus time (a) and carbon conversion (Xg) versus time for pine wood chip (PWC) char combustion (b). Experimental data from Ammendola et al., 2013.

In order to further validate the combustion-attrition particle model, the predictions are compared against the results from Chirone et al, 2006[33] which utilized both the same pine wood chip (PWC) feedstock and experimental setup. However, in this case the oxygen concentration was varied (1-21% vol. oxygen) and a higher reactor temperature was adopted (850°C instead of 800°C). The model inputs were modified to reflect these changes in reactive conditions and a fragmentation factor of n_1=3 was assumed. Figure 7 shows the apparent char conversion (X_m) versus time for the various oxygen concentrations tested. It should be noted that this definition of char conversion (X_m) represents the conversion of the char by all pathways (combustion and attrition) and therefore, by definition, approaches 1 in all cases. The actual carbon conversion (X_g) representing the conversion due to combustion was not published by the original authors.

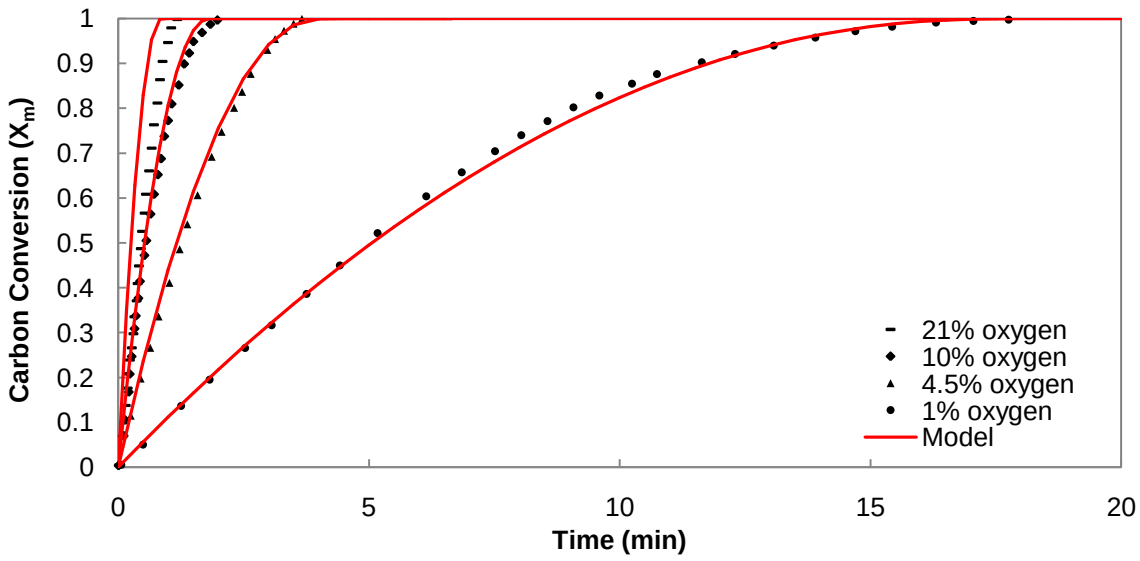

Figure 7 Apparent char conversion (X_m) versus time for pine wood chip (PWC) char combustion (b) at 850 °C. Experimental data from Chirone et al., 2006[33]

The model and experimental data appear to agree extremely well. Both show a clear inverse relationship between oxygen concentration (1%, 4.5%, 10%, and 21% vol oxygen) and burnout

time (15.67, 5.38, 3.65, 1.63, and 0.8) minutes for the respective oxygen concentrations. Predicted burnout times are within 30 seconds of the experimentally reported burnout times. For the 21% oxygen condition, the model predicts a shorter burnout time of 0.8 minutes compared to the experimentally reported time of 1.12 min. However this represents an absolute difference of only 20 seconds. No experimental uncertainties or error bounds were provided but it is likely within the uncertainties of the both the experiment and modeling approach.

The model predicts asymptotic carbon conversions (X_g) of (96%, 99.1%, 99.5%, and 99.7%) increasing with oxygen concentration (1%, 4.5% 10%, and 21% vol), respectively. As mentioned, the actual carbon conversion (X_g) profiles were not reported experimentally; however, it was stated that conversions higher than 97% were achieved for all tested oxygen concentrations- agreeing with the model predictions.

3.3.Continuously-fed (steady-state) model

Under most experimental or industrial conditions, gasifiers and combustors are continuously fed with fresh biomass, and as a result, char particles are constantly generated via devolatilization. Operated this way, the reactor may be initially empty of char but eventually reaches a steady-state inventory of char over a period of time which can take several hours[63]. A *steady state* model is now presented which predicts the behavior (char inventory, average char residence time and reaction rates) of such continuously fed reactors under a specified biomass feed rate, temperature, pressure, and reactive conditions. The approach considers that a distribution of particles (with varying ages) exists in the reactor and by suitably averaging the transient model results, relevant statistics for the distribution of particles can be solved for. Perhaps most importantly, the steady state inventory of char $m_{ch,ss}$ is not known *a priori* and must be

predicted. By applying a mass balance across the gasifier, the char produced by devolatilization must be balanced by the consumption of char through gasification, attrition/elutriation, and combustion[5,19] ,

$$0 = \dot{m}_f Y_{ch} - (\bar{R}_{gasi} + \bar{R}_{attr} + \bar{R}_{comb})m_{ch,ss} \tag{43}$$

where, because a distribution of particles exists, $\bar{R}$ represents a residence time mass-averaged rate (1/s) over all the char particles in the gasifier. Combining this equation with the definition of average residence time in equation (4) enables the average residence time to be written in terms of these rates,

$$\bar{\tau}_{ch} = 1/\left(\bar{R}_{gasi} + \bar{R}_{attr} + \bar{R}_{comb}\right) \tag{44}$$

Since the rates of gasification and attrition are not necessarily constant over the course of conversion, it is necessary to perform a residence time mass-weighted average of each rate $\bar{R}(\tau)$ (1/s) from the transient particle model

$$\bar{R}(\tau) = \int_0^\infty \tilde{R}\,(t)E(t,\tau)dt \tag{45}$$

$$\tilde{R}(t) = 1/t \int_0^t R(t)dt \tag{46}$$

$$t = t_c \; for \; t > t_c$$

where, $\tilde{r}(t)$ is a time-averaged rate (1/s), and $E(t,\tau)$ is the dimensionless exit age distribution function and t_c is the time to reach complete conversion (i.e. $X_m(t_c)$=1). The conditional statement in equation (46) reflects that the fact the time-averaged rate should be invariant for conversion beyond unity X_m=*1*. For a well-stirred reactor, particles exhibit the following residence time distribution.

$$E_{WSR}(t,\tau) = \exp(-t/\tau)/\tau \quad (47)$$

It has been verified experimentally that char remains well-mixed in a fluidized bed gasifier[18]; however, the numerical solution of the model enables an arbitrary RTD to be employed.

The solution procedure for the steady state model is as follows: the transient model ODE's are solved until full conversion is reached $X_m=1$ and time-averaged rates equation (46) can be computed for all times, ($0<t\leq t_c$). Since, the average residence time given in equation (44) is implicitly defined, an initial guess for $\bar{\tau}_{ch}$ is substituted into equation (47), which results in a new guess for the average residence time. The new guess is re-substituted and this process is iterated until τ_{ch} converges to a value. The same iterative process is used to compute the residence time and steady state inventory of ash.

3.3.1. Impact of gasification temperature on char conversion

The steady state model was setup to describe a continuously fed reactor with reactive environment of steam (30%vol), carbon dioxide (30%vol) and nitrogen (40%vol) at varying temperatures between 700 to 900°C. Other reactor properties such as the bed material, fluidizing conditions, and feedstock properties (summarized in Table 5), are unchanged from the previous section. The results in Figure 8 demonstrate that the steady state average char conversion ($X_{g,ss}$) increases with temperature as expected while the residence time of the char particles reduces dramatically. The sensitivity of char conversion to temperature is mostly linear between 700-850°C: a 50K increase in temperature results in a 15% (wt. initial char) increase in conversion. This also shows the importance of having a model which predicts the char inventory and average residence time, as these quantities vary significantly over typical operating temperatures. They

cannot be assumed to be constant. Interestingly, the model predicts that PWC exhibits consistently lower steady state conversion compared to the SWP, primarily due to its higher attrition behavior. This provides further justification for feedstock pre-treatment as a useful technology- especially for non-woody feedstocks, which would be expected to have even less favorable attrition characteristics.

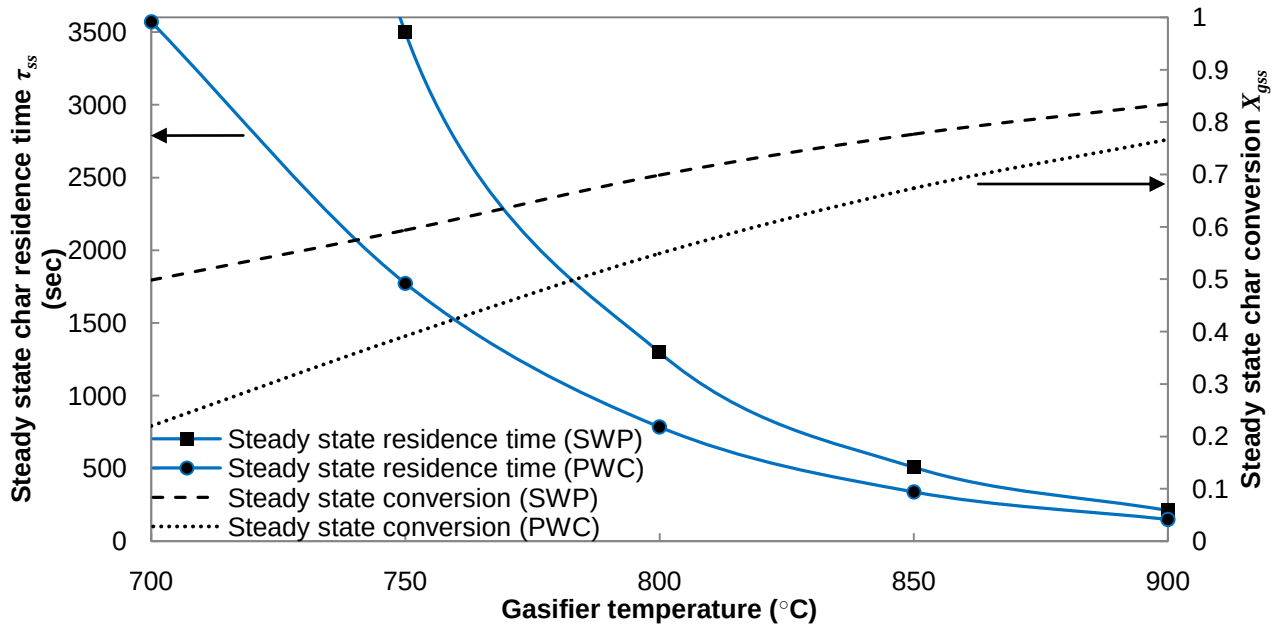

Figure 8. Average steady state char residence time $\tau_{ch,ss}$ (seconds) (left axis) versus temperature (°C) and average steady state char conversion, $X_{g,ss}$ (right axis) for SWP and PWC feedstocks

The model results in Figure 8 have several implications for actual gasifier operation. The model provides a quantitative explanation of the previously observed experimental conclusions regarding the difficulty of achieving high steady state char conversion in a single-stage gasifier[6]. Even as the temperature of the gasifier is raised, the char residence time decreases due to the

competing effect of attrition/elutriation. At the highest reactor temperature (900°C) the steady state spruce wood pellet conversion is still only 83.4% and 76.6% for the pine wood char.

Another important application of this model concerns the issue of bed inventory. Since the average residence time increases with decreasing temperature, so does the steady state inventory of char in the bed (see equation (4)). Due to the low effective density of char, excessive buildup of char in the bed will at some point impede proper fluidization and mixing leading to operational problems requiring a lower feed rate or ash removal- especially if the feedstock has a high-ash content[5]. By applying a hypothetical criteria that the steady state volume of char must be less than 10% the volume of the entire bed, one can compute the maximum char feed rate for a given reactor bed volume,

$$\dot{m}_{ch,max} < 0.1 \frac{\rho_{ch,ss} \varepsilon_{ch,bed} V_{bed}}{\tau_{ch,ss}(T,P)}$$

This relationship demonstrates important relationships between feed rate and residence time. The longer the residence time needed to convert a feedstock, the lower the maximum stable feeding rate. Intuitively, for a given operating temperature and feedstock, the throughput of a reactor can be increased by building a larger reactor. Taking a 3 meter diameter reactor with 1 meter high bed material as a characteristic size for an industrial scale fluidized bed reactor[64], and further substituting values for the char packing fraction, $\varepsilon_{ch,bed} = 0.4$, and density $\rho_{ch,ss} = 150$ kg/m^3, the maximum char feed rate can be computed versus temperature by substituting the computed steady state residence times. At 700 °C such a reactor could only process <14kg$_{char}$/hr while at 900°C it could process <726kg$_{char}$/hour, a factor of more than 50 higher.

One potentially desirable approach to increase the throughput would be to elevate the operating pressure. In Figure 9 the steady state residence time and char conversion are plotted versus operating pressure at a fixed operating temperature of 800°C. The results show that the

char conversion is not increased significantly at elevated pressures. At 1atm abs the SWP demonstrates a steady state conversion of 70% while at 20 atm abs this only marginally increases to 71%. This can be explained by the magnitude of the denominator term in the Langmuir-Hinshelwood kinetics. However, as shown in Table 3, the original kinetics were only fitted at atmospheric pressure with a maximum steam partial pressure of 1 bar atm[19], so their validity at these high pressures is not known.

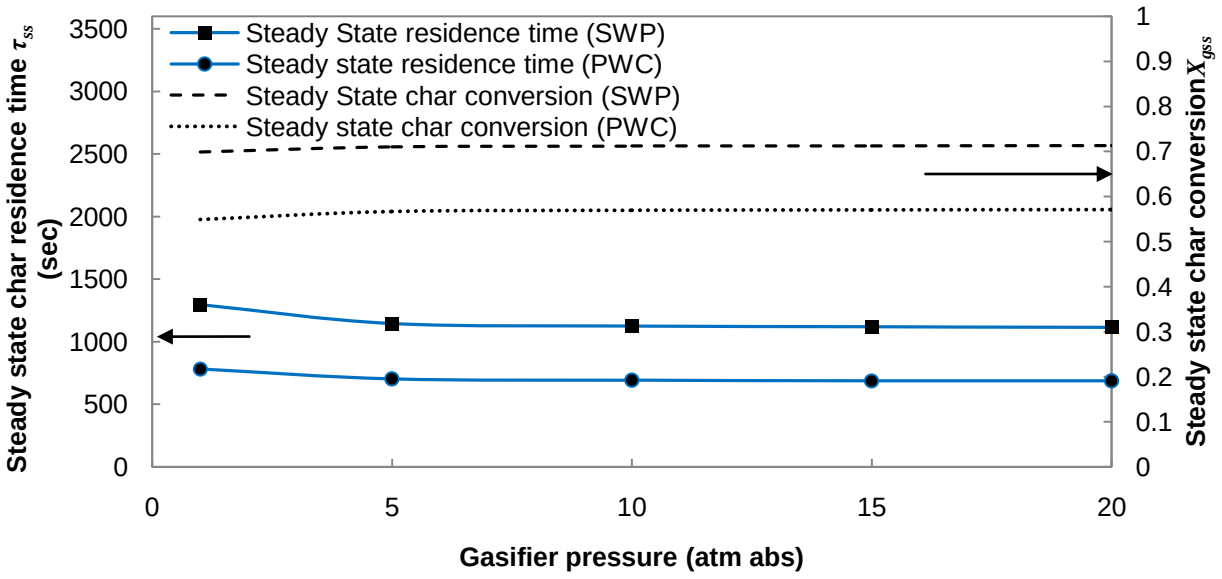

Figure 9 Average steady state char residence time τ_{ch} (seconds) (left axis) versus gasifier pressure (atm) and average steady state char conversion, X_g (right axis) for T=800 °C

In order to understand the sensitivity of the steady state model results to the input and fitted parameters a local sensitivity analysis is performed. Temperature and pressure are fixed at 800°C and 1atm, respectively, while the three fitted parameters, (K_{att0}, ψ, and q), two feedstock dependent parameters (n_1, d_f) and the superficial gas velocity (u_0) are varied by ±20% around the base values summarized in Table 5. The results shown in Figure 10a,b demonstrate that of the parameters considered, the structural attrition parameter, q has the largest effect on steady state

char conversion. A 20% increase in q results in a 5% reduction in steady state char conversion. It is important that robust feedstock-dependent attrition model parameters (K_{att0} and q) be fitted with batch gasification/attrition data[14] in order to accurately predict of char conversion. In order to maximize char conversion, the reactor should be operated at a low superficial gas velocity, and feedstocks demonstrating a large initial particle size, high reactivity, and low initial attrition constant should be utilized.

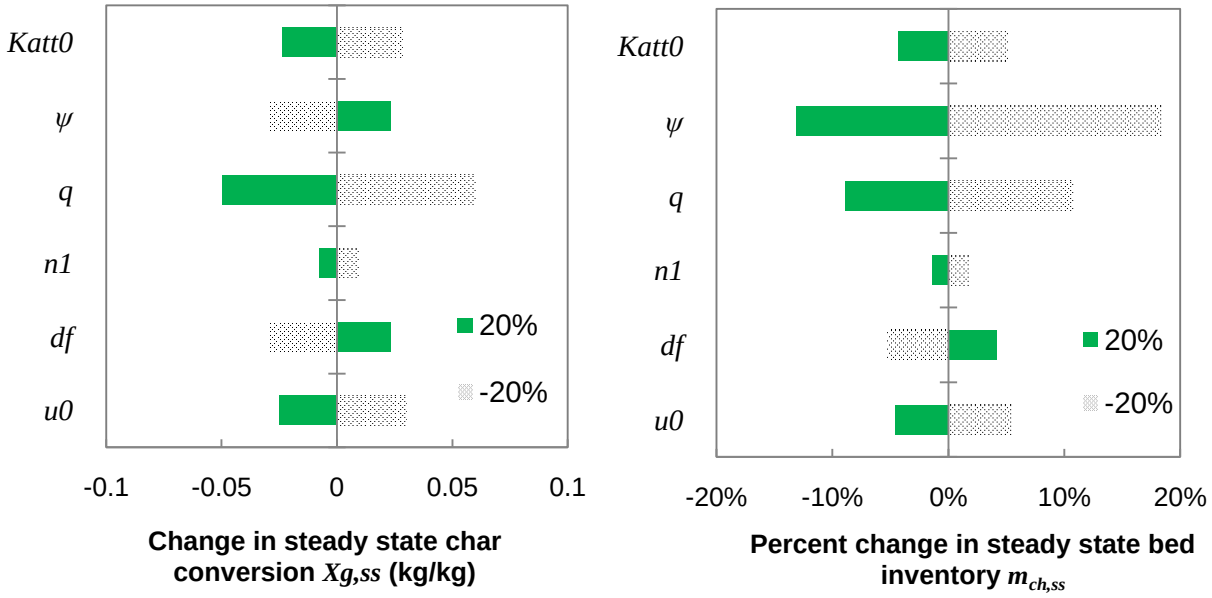

Figure 10a,b Local sensitivity of fitted and input parameters on $X_{g,ss}$ and $m_{ch,ss}$, respectively for PWC char gasification. (T=1073K, P=101325Pa, X_{H2O}=0.3, X_{CO2}=0.3, and X_{N2}=0.4)

The adjusted reactivity parameter, ψ, has the largest impact on the steady state bed inventory. A 20% increase in the reactivity results in 13% reduction in the steady state bed inventory. This demonstrates the importance of accurately quantifying the char reactivity, which is still under investigation by many researchers. The primary fragmentation factor (n_1) is shown to have a minimal effect on either char conversion or steady state inventory under gasification conditions.

3.4.Model limitations and future work

A gasification-assisted attrition structural profile was proposed and fitted under CO_2 gasification conditions, but future work should consider conditions where combinations of steam, carbon dioxide, and oxygen are injected during batch experiments in order to verify that the gasification/oxidizing agent does not impact the fitted structural attrition profile. Additional data for the secondary fragmentation of biomass chars under gasification conditions would further elucidate the mechanisms of gasification-assisted attrition- eventually allowing this effect to be quantitatively incorporated into models.

The combustion of fines was neglected in this case but may be significant in cases where the oxygen concentration is higher. Also, if the bed is operated at low enough superficial gas velocities the fines may have a longer residence time and -depending on the availability of oxygen- further combust. The elutriation of mother particles was also assumed to be negligible in the cases studied. However, if smaller (or less dense) initial char particles are generated or significantly higher gas velocities are employed, this assumption may no longer hold. The characteristic time analysis shown in Table is a useful methodology and should be used to verify whether these phenomena should be included for the specific cases under consideration.

Future work aims to couple this steady-state char conversion model with a separate reactor-scale model[25] for the gas phase reactions in the fluidized bed. Coupling these models will enable a robust prediction for the quantities of steam, carbon dioxide, and oxygen that react with char under steady operating conditions.

4. Conclusions

A transient particle model to describe char conversion of biomass under fluidized bed gasification and combustion conditions has been developed. A novel structural attrition function was introduced to account for gasification-assisted attrition during gasification. A comprehensive model for char combustion which accounted for internal, external, and kinetic limitations was presented and validated again published experimental data. Wood chip chars were found to demonstrate much higher initial attrition rate than spruce pellet chars but the hardness of both feedstocks deteriorates rapidly with increasing conversion. The combustion behavior of both feeds are highly dependent on particle size/geometry due to the strong presence of mass transfer limitations. Wood chip chars combust significantly faster than spruce pellets due to the lower density and size. The results are extended to a continuously fed steam/CO_2 gasifier to elucidate the impact of increasing temperature and pressure on steady state char conversion. It is found that as the temperature is raised, char reactivity also increases but gasification-assisted attrition acts to shorten the residence time of the char particles making complete char conversion (X_g=1) impossible. Steady state char conversion is found to be more sensitive to temperature than pressure due to the strong effects of inhibition. As a result, elevated pressures demonstrate little impact improving steady state conversion. Lastly, the model provides a rigorous way to estimate appropriate biomass feed rates as a function of temperature, pressure, reactor volume, and feedstock- highly useful for scaling and design studies

Appendix: Char combustion

Reaction stoichiometry

The combustion reaction of carbon can be written generally with a stoichiometric coefficient (also referred to as a product distribution coefficient) λ[65] ,

$$C + \lambda O_2 \rightarrow (2 - 2\lambda)CO + (2\lambda - 1)CO_2$$

The assumed coefficient can vary between 0.5 and 1, yet the literature provides no clear agreement on the appropriate value for λ under fluidized bed gasification conditions. For this study, it was assumed that $\lambda = 0.5$ which is supported by several models[24,66,67] and experiments[68] in the literature.

Size and geometry characterization

Table 6 Particle geometry definitions

	Aspect ratio	**Volume/surface diameter $d_{p,VS}$**	**Sphericity Ψ**
Finite cylinder of diameter, $d_{p,cyl}$ and length, L_p	$AR_{cyl} = \frac{L_p}{d_{p,cyl}}$	$d_{p,VS} = \frac{6d_{p,cyl}}{(2d_{p,cyl}/L_p + 4)} = \frac{6d_{p,slb}}{2/AR_{cyl} + 4}$	$\Psi_{cyl} = \frac{(3/2)^{2/3} AR_{cyl}{}^{2/3}}{1/2 + AR_{cyl}}$
Finite square slab of thickness t_p and width $d_{p,slb}$	$AR_{slb} = \frac{d_{p,cyl}}{t_p}$	$d_{p,VS} = \frac{6}{2/t_p + 4/d_{p,slb}} = \frac{6d_{p,slb}}{2AR_{slb} + 4}$	$\Psi_{slb} = \frac{6^{2/3}\pi^{1/3} AR_{slb}{}^{1/3}}{2AR_{slb} + 4}$

Effectiveness factors

Internal effectivenesss factor

The quasi-steady state species conservation equation for reaction in a spherical porous medium,

$$\frac{D_{eff}}{{R_p}^2}\frac{d}{dr}\left({R_p}^2\frac{dC_{O_2}}{dr}\right)-k_{O_2}C_{O_2}C_c\lambda=0 \tag{48}$$

where, $R_p=d_p/2$ is the particle radius for the spherically equivalent particle with the same volume to surface ratio as the particle. The solution to this steady state differential equation can be solved subject to the following boundary conditions: there exists symmetry at the particle center (Neumann), (r=0) and the oxygen concentration at the surface is specified (Dirchlet) C_s (r=R_p),

$$C_{O_2}=C_s\frac{R_p}{r}\frac{e^{\gamma r}-e^{-\gamma r}}{e^{\gamma R_p}-e^{-\gamma R_p}}=C_s\frac{R_p}{r}\frac{\sinh(\gamma r)}{\sinh(\gamma R_p)} \tag{49}$$

Where an inverse penetration length, γ with units of (1/m) is defined,

$$\gamma=\sqrt{k_{O_2}C_c\lambda/D_{eff}} \tag{50}$$

The internal effectiveness factor, η_{int}, can be defined as the actual reaction rate divided by the reaction rate if the entire particle had a uniform concentration across it. The actual reaction rate can be computed by the flux of oxygen $J_{particle}$ to the surface of the particle, which by Fick's law, depends on the gradient of oxygen concentration at the surface (r=R_p).

$$J_{particle}=-D_{eff}\left.\frac{dC_{O_2}}{dr}\right|_{r=R_p} \tag{51}$$

Thus the η_{int} can be written in terms of known quantities,

$$\eta_{int}=\frac{4\pi{R_p}^2J_{particle}}{\frac{4}{3}\pi{R_p}^3kC_sC_c\lambda}=\frac{3}{\gamma R_p}\left(\frac{1}{\tanh(\gamma R_p)}-\frac{1}{\gamma R_p}\right) \tag{52}$$

Now defining the Thiele modulus as,

$$\phi=\gamma R_p/3 \tag{53}$$

then, the internal effectiveness factor can be written in its commonly published form,

$$\eta_{int} = \frac{1}{\phi}\left(\frac{1}{\tanh(3\phi)} - \frac{1}{3\phi}\right) \tag{54}$$

Note that the dimensionless Thiele modulus can be interpreted as a Damkolher number relating the time scale of diffusion divided by the time scale of chemical reaction,

$$Da_{int} = \phi^2 = \left(\frac{d_p^2}{36D_{eff}}\right)\left(k_{O_2} C_c \lambda\right) = \frac{\tau_{int,diff}}{\tau_{rxn}} \tag{55}$$

External effectiveness factor

The actual oxygen concentration at the particle surface depends on external mass transfer limitations. By mass conservation, the flux at the surface of the particle must be equal to the flux through the boundary layer,

$$J_{particle} = h_m(C_s - C_b) \tag{56}$$

Where C_b is the concentration of oxygen in the bulk. Solving for the actual concentration at the particle surface,

$$C_s = \frac{C_b}{\eta_{int}\phi_{ext} + 1} \tag{57}$$

Where the external Thiele modulus can be defined,

$$\phi_{ext} = \frac{d_p k_{O_2} C_c \lambda}{6h_m} \tag{58}$$

Likewise, an external Dahmkohler number can be defined from the external Thiele modulus,

$$Da_{ext} = \phi_{ext}^2 = \left(\frac{d_p^2}{6ShD_{eff}}\right)\left(k_{O_2} C_c \lambda\right) = \frac{\tau_{ext,diff}}{\tau_{rxn}} \tag{59}$$

Finally, the external effectiveness factor η_{ext} is defined as the actual reaction rate divided by the rate if the particle surface was the same as the bulk concentration,

$$\eta_{ext} = \frac{1}{\eta_{int}\phi_{ext} + 1} \tag{60}$$

Conversion-averaged combustion properties

Certain distinctions must be made when applying the effectiveness factor approach to reacting char particles. Unlike catalyst particles whose properties are relatively constant during a reaction, char particles are consumed during their reaction[55]. Therefore, the pore structures are neither uniform initially, nor constant during the particle's conversion. As a result, a variation in both the reactivity and effective diffusivity of reactants through the particle must be accounted for. If combustion is considered to occur completely over a relatively thin zone in the particle, the average properties across this front should be constant during the consumption of the particle[56]. This variation can be included by using conversion-averaged properties for the combustion rate,

$$\hat{r}_{comb} = r_{O_2} \int_0^1 F_{O_2}(X_\rho) dX \tag{61}$$

and for the effective diffusivity,

$$\widehat{D}_{eff} = D_{binary} \int_0^1 D_{eff}(X_\rho) dX \tag{62}$$

where, in the latter it helps to define the conversion X_ρ in terms of the void fraction,

$$X_\rho = \frac{\varepsilon_g - \varepsilon_{g,0}}{1 - \varepsilon_{g,0}} \tag{63}$$

Apparent combustion kinetic representation

It is common to represent the effective rate as a series combination of apparent internal kinetic-diffusion resistance and an external diffusion resistance. This is usually applied when the combustion of the entire char solid phase is considered in an average sense[44]. The overall effective rate of oxygen consumption $mol_{O2}/m^3_{particle}/sec$ per unit volume of solid phase can be written,

$$R_{comb,eff} = kC_s C_c \lambda \eta_{int} \tag{64}$$

Substituting the steady state concentration of oxygen at the surface C_s from equation (57) this can be re-written as,

$$R_{comb,eff} = \frac{C_b}{\frac{d_p}{6}\left(\frac{1}{h_m} + \frac{6}{d_p D_{eff} \gamma^2 \eta_{int}}\right)} = \frac{C_b}{\frac{d_p}{6}\left(\frac{1}{h_m} + \frac{1}{k_{rm}}\right)} \quad (65)$$

where the rate is represented by two series resistances with units of s/m. This expression enables the apparent kinetic-diffusion limitation to be written as a function of both feedstock and reactor properties. The second term in the denominator, k_{rm} with units of m/s is commonly referred as the surface burning rate and can be more simply expressed under the assumption that the internal diffusion resistance is much higher than the kinetic resistance ($\phi > 3$).

$$k_{rm} = \frac{d_p D_{eff} \gamma^2 \eta_{int}}{6} = \sqrt{k_{O_2} C_c D_{eff} \lambda} \quad (66)$$

Substituting the conversion averaged reactivity and diffusivity for PWC and SWP into this expression, the surface burning rate (m/s) can be written,

$$k_{rm} = A_1 \exp\left(-\frac{6539}{T}\right) T^{1.375} P^{-0.5} \lambda^{0.5} \quad (67)$$

where A_1 is 3.06 for PWC and 4.4 ($m^{-0.5}s^{-2}kg^{0.5}K^{-1.375}$) for SWP.

AUTHOR INFORMATION

Corresponding Author

*Corresponding Author Email: rbates@mit.edu

Author Contributions

The manuscript was written through contributions of all authors. All authors have given approval to the final version of the manuscript.

Funding Sources

Acknowledgement

The authors gratefully acknowledge BP for funding this research. This research was supported in part by an appointment to the National Energy Technology Laboratory Research Participation Program, sponsored by the U.S. Department of Energy and administered by the Oak Ridge Institute for Science and Education. They also would like to thank Amelia Brooks for her help during the initial screening of transport-kinetics correlations.

Nomenclature

Nomenclature			
Notation		*Greek letters*	
		γ	inverse penetration length (1/m)
A	pre-exponential factor (s^{-1})	ε_j	volume fraction ($m^3_j/m^3_{particle}$)
AR	Aspect ratio ()	η	effectiveness factor ()
C	concentration ($mol/m^3/s$)	κ	Inhibition kinetics parameter
		λ	Stoichiometric coefficient ($mol_{O2}/mol_{C)}$
d_p	particle volume/surface mean diameter	μ_f	dynamic viscosity (Pa-s)
D	diffusivity (m^2s^{-1})	ρ	density (kg/m^3)
E	exit age distribution	σ	constriction factor ()
F	structural profile ()	τ	residence time or time-scale (sec)
h_m	mass transfer coefficient (m/s)	τ_p	tortuosity ()
J	molar flux ($mol/m^2/sec$)	φ_s	shrinkage factor ($m^3_{particle,biomass}/m^3_{particle,char}$)
k_{O_2}	kinetics constant in eq. (27) ($m^3/mol_{O2}/sec$)	ϕ	Thiele modulus ()
k_{rm}	combustion burning rate (m/s)	ψ	reactivity factor ()
k_j	kinetics constant in eq. (19)-(21) ($bar^{-n}sec^{-1}$)	Ψ	sphericity ()
K	attrition constant ()		
L_p	cylinder length scale (m)	*Subscripts*	
m	particle mass (kg)	*att*	attrition
MW	atomic weight ($kg\ mol^{-1}$)	*b*	bulk
n	number of particles	*bio*	biomass
n_1	primary fragmentation factor ()	*c*	carbon
n_2	Secondary fragmentation factor ()	*ch*	char
p	Pressure (bar)	*cyl*	cylinder
P	pressure (Pa)	*comb*	combustion
q	attrition structural factor ()	*ext*	external
r_j	rate of j (1/s)	*eff*	effective
R_j	Reactivity or rate (1/s)	*f*	fuel/feed
R_p	particle size (radius) (m)	*g*	gas (void)
R_g	universal gas constant ($J\ mol^{-1}K^{-1}$)	*gasif*	gasification
T	temperature (K)	*int*	internal
t	time (s)	*s*	surface
t_p	flake length scale (m)	*slb*	slab
V	volume (m^3)	*ss*	steady state
X	conversion (-)	*0*	initial
u_0	superficial gas velocity (m/s)		
u_{mf}	minimum fluidizing velocity (m/s)		
Y_j	yield from biomass ($kg_j/kg_{biomass}$)		

ABBREVIATIONS

FBBG, fluidized bed biomass gasification; BFB bubbling fluidized bed; BTL biomass to liquids, PWC pine wood chip, SWP, spruce wood pellet,

REFERENCES

(1) Dupont, C.; Boissonnet, G.; Seiler, J.-M.; Gauthier, P.; Schweich, D. *Fuel* **2007**, *86* (1-2), 32–40.
(2) Moilanen, A.; Nasrullah, M.; Kurkela, E. *Environ. Prog. Sustain. Energy* **2009**, *28* (3), 355–359.
(3) Milne, T. .; Evans, R. J.; Abatzoglou, N. *Biomass gasifier "tars": Their nature, formation and conversion*; TP-570-25357; National Energy Technology Laboratory (NETL): Boulder, CO, 1998.
(4) Göransson, K.; Söderlind, U.; He, J.; Zhang, W. *Renew. Sustain. Energy Rev.* **2011**, *15* (1), 482–492.
(5) Gómez-Barea, A.; Leckner, B. *Fuel* **2013**, *107* (0), 419–431.
(6) H. Thunman; Seemann, M. C. In *Proceedings of the 20th International Conference on Fluidized bed Combustion*; Springer-Verlag: Xi'an, 2010; pp 659–663.
(7) Kurkela, E.; Staåhlberg, P. *Fuel Process. Technol.* **1992**, *31* (1), 23–32.
(8) Heidenreich, S.; Foscolo, P. U. *Prog. Energy Combust. Sci.* **2015**, *46*, 72–95.
(9) Gomez-Barea, A.; Leckner, B. *Prog. Energy Combust. Sci.* **2010**, *36* (4), 444–509.
(10) Guizani, C.; Escudero Sanz, F. J.; Salvador, S. *Fuel* **2013**, *108* (0), 812–823.
(11) Hognon, C.; Dupont, C.; Grateau, M.; Delrue, F. *Bioresour. Technol.* **2014**, *164* (0), 347–353.
(12) Umeki, K.; Moilanen, A.; Gómez-Barea, A.; Konttinen, J. *Chem. Eng. J.* **2012**, *207–208* (0), 616–624.
(13) Di Blasi, C. *Prog. Energy Combust. Sci.* **2009**, *35* (2), 121–140.
(14) Ammendola, P.; Chirone, R.; Ruoppolo, G.; Scala, F. *Proc. Combust. Inst.* **2013**, *34* (2), 2735–2740.
(15) Troiano, M.; Ammendola, P.; Scala, F. *Proc. Combust. Inst.* **2013**, *34* (3), 2741–2747.
(16) Beer, J. M.; Massimilla, L.; Sarofim, A. F. *Proc. Int. Conf. Fluid. Bed Combust. Syst. Appl. Inst. Energy Symp. Ser. No 4* **1980**.
(17) Konttinen, J. T.; Moilanen, A.; DeMartini, N.; Hupa, M. *Biomass Convers. Biorefinery* **2012**, *2* (3), 265–274.
(18) Nilsson, S.; Gómez-Barea, A.; Fuentes-Cano, D.; Ollero, P. *Fuel* **2012**, *97*, 730–740.
(19) Kramb, J.; Konttinen, J.; Gómez-Barea, A.; Moilanen, A.; Umeki, K. *Fuel* **2014**, *132* (0), 107–115.
(20) Natale, G.; Galgano, A.; Di Blasi, C. *Biomass Bioenergy* **2014**, *62* (0), 123–137.
(21) Scala, F.; Salatino, P. *Chem. Eng. Sci.* **2002**, *57* (7), 1175–1196.
(22) Khan, A. A.; De Jong, W.; Gort, D. R.; Spliethoff, H. *Energy Fuels* **2007**, *21* (4), 2346–2356.
(23) Kaushal, P.; Abedi, J.; Mahinpey, N. *Fuel* **2010**, *89* (12), 3650–3661.
(24) Galgano, A.; Di Blasi, C.; Horvat, A.; Sinai, Y. *Energy Fuels* **2006**, *20* (5), 2223–2232.

(25) Stark, A. K.; Bates, R. B.; Zhao, Z.; Ghoniem, A. F. *Energy Fuels* **2015**, *29* (4), 2437–2452.
(26) Goossens, W. R. . *Powder Technol.* **1998**, *98* (1), 48–53.
(27) Colakyan, M.; Levenspiel, O. *Powder Technol.* **1984**, *38* (3), 223–232.
(28) Lin, L.; Sears, J. T.; Wen, C. Y. *Powder Technol.* **1980**, *27* (1), 105–115.
(29) Mandl, C.; Obernberger, I.; Biedermann, F. *Fuel* **2010**, *89* (12), 3795–3806.
(30) Arena, U.; D'Amore, M.; Massimilla, L. *AIChE J.* **1983**, *29* (1), 40–49.
(31) Ray, Y. C.; Jiang, T. S.; Wen, C. Y. *Powder Technol.* **1987**, *49* (3), 193–206.
(32) Chirone, R.; Salatino, P.; Scala, F.; Solimene, R.; Urciuolo, M. *Combust. Flame* **2008**, *155* (1–2), 21–36.
(33) Scala, F.; Chirone, R.; Salatino, P. *Energy Fuels* **2006**, *20* (1), 91–102.
(34) Dennis, J. S.; Hayhurst, A. N.; Scott, S. A. *Combust. Flame* **2006**, *147* (3), 185–194.
(35) Cano, G.; Salatino, P.; Scala, F. *Fuel Process. Technol.* **2007**, *88* (6), 577–584.
(36) Gomez-Barea, A.; Leckner, B.; Campoy, M. In *Proceedings of the 9th International Conference on Circulating Fluidized Beds*; Werther, J., Nowak, W., Hartge, E.-U., Eds.; Hamburg, Germany, 2008; pp 727–732.
(37) Basu, P.; Subbarao, D. *Combust. Flame* **1986**, *66* (3), 261–269.
(38) Gómez-Barea, A.; Ollero, P.; Fernández-Baco, C. *Energy Fuels* **2006**, *20* (5), 2202–2210.
(39) Moilanen, A.; Saviharju, K. In *Developments in Thermochemical Biomass Conversion*; Bridgwater, A. V., Boocock, D. G. B., Eds.; Springer Netherlands, 1997; pp 828–837.
(40) Risnes, H.; Sørensen, L. H.; Hustad, J. E. In *Progress in Thermochemical Biomass Conversion*; Blackwell Science Ltd, 2001; pp 61–72.
(41) Barrio, M. Experimental Investigation of Small-scale Gasification of Woody Biomass. Ph.D. thesis, Norwegian University of Science and Technology: Trondheim, Norway, 2002.
(42) Moilanen, A. Thermogravimetric characterisations of biomass and waste for gasification processes. PhD. Thesis, Åbo Akademi University: Espoo, 2006.
(43) Li, J.; Bonvicini, G.; Biagini, E.; Yang, W.; Tognotti, L. *Fuel* **2015**, *143* (0), 492–498.
(44) Gerber, S.; Behrendt, F.; Oevermann, M. *Fuel* **2010**, *89* (10), 2903–2917.
(45) Cooper, J.; Hallett, W. L. H. *Chem. Eng. Sci.* **2000**, *55* (20), 4451–4460.
(46) Xue, Q.; Fox, R. O. *Powder Technol.* **2014**, *254*, 187–198.
(47) Hobbs, M. L.; Radulovic, P. T.; Smoot, L. D. *AIChE J.* **1992**, *38* (5), 681–702.
(48) Field, M. A.; Gill, D. W.; Morgan, B. B.; Hawksley, P. G. W. *Combustion of Pulverised Fuel*; British Coal Utilisation Research Association: Leatherhead, Surrey, 1967.
(49) Di Blasi, C.; Buonanno, F.; Branca, C. *Carbon* **1999**, *37* (8), 1227–1238.
(50) Sun, J.-K.; Hurt, R. H. *Proc. Combust. Inst.* **2000**, *28* (2), 2205–2213.
(51) Dennis, J. S.; Lambert, R. J.; Milne, A. J.; Scott, S. A.; Hayhurst, A. N. *Fuel* **2005**, *84* (2–3), 117–126.
(52) Niu, Y.; Shaddix, C. R. *Proc. Combust. Inst.* **2015**, *35* (1), 561–569.
(53) Wijngaarden, R. J.; Kronberg, A.; Westerterp, R. *Industrial Catalysis: Optimizing Catalysts and Processes*; Wiley-VCH Verlag GmbH, 1998.
(54) Ollero, P.; Serrera, A.; Arjona, R.; Alcantarilla, S. *Fuel* **2002**, *81* (15), 1989–2000.
(55) Prins, W. J.; Van Swaaij, W. P. M. In *Fluidized bed Combustion*; Radovanovic, M., Ed.; Proceedings of the International Centre for Heat and Mass Transfer; Hemisphere Publishing Corporation, 1986; pp 165–184.

(56) Szekely, J.; Evans, J. W.; Sohn, H. Y. In *Gas-Solid Reactions*; Academic Press Inc.: New York, NY, 1976.
(57) Di Blasi, C. *Chem. Eng. Sci.* **2000**, *55* (15), 2931–2944.
(58) *Fluidized bed technologies for near-zero emission combustion and gasification*; Scala, F., Ed.; Woodhead Publishing Series in Energy; Woodhead Publishing: Cambridge, UK, 2013.
(59) Scala, F. *Chem. Eng. Sci.* **2007**, *62* (16), 4159–4176.
(60) Ragland, K. W.; Aerts, D. J.; Baker, A. J. *Bioresour. Technol.* **1991**, *37* (2), 161–168.
(61) Purnomo; Ragland, K. W.; Aerts, D. J. *Twenty-Third Symp. Int. Combust.* **1991**, *23* (1), 1025–1032.
(62) Wen, C. Y.; Yu, Y. H. *AIChE J.* **1966**, *12* (3), 610–612.
(63) Valin, S.; Ravel, S.; Guillaudeau, J.; Thiery, S. *Fuel Process. Technol.* **2010**, *91* (10), 1222–1228.
(64) Werther, J. *Chem. Eng. Sci.* **1992**, *47* (9–11), 2457–2462.
(65) Yan, H.; Zhang, D. *Chem. Eng. Process. Process Intensif.* **2000**, *39* (3), 229–237.
(66) Chen, L.; Yong, S. Z.; Ghoniem, A. F. *Prog. Energy Combust. Sci.* **2012**, *38* (2), 156–214.
(67) Ross, I. B.; Davidson, J. F. *Trans. Inst. Chem. Eng.* **1982**, *60*, 108–114.
(68) Hayhurst, A. N.; Parmar, M. S. *Chem. Eng. Sci.* **1998**, *53* (3), 427–438.